

# 000 SYMMETRIC PRUNING FOR LARGE LANGUAGE MOD- 001 002 ELS 003 004

005 **Anonymous authors**

006 Paper under double-blind review

## 007 008 ABSTRACT 009

010 Popular post-training pruning methods such as Wanda (Sun et al., 2023) and  
011 RIA (Zhang et al., 2024b) are known for their simple, yet effective, designs that  
012 have shown exceptional empirical performance. Wanda optimizes performance  
013 through calibrated activations during pruning, while RIA emphasizes the relative,  
014 rather than absolute, importance of weight elements. Despite their practical suc-  
015 cess, a thorough theoretical foundation explaining these outcomes has been lack-  
016 ing. This paper introduces new theoretical insights that redefine the standard mini-  
017 mization objective for pruning, offering a deeper understanding of the factors con-  
018 tributing to their success. Our study extends beyond these insights by proposing  
019 complementary strategies that consider both input activations and weight signifi-  
020 cance. We validate these approaches through rigorous experiments, demon-  
021 strating substantial enhancements over existing methods. Furthermore, we introduce  
022 a novel training-free fine-tuning approach  $R^2$ -DSnoT that incorporates relative  
023 weight importance and a regularized decision boundary within a dynamic pruning-  
024 and-growing framework, significantly outperforming strong baselines and estab-  
025 lishing a new state-of-the-art.

## 026 027 1 INTRODUCTION

028 Large Language Models (LLMs) (Zhang et al., 2022a; Touvron et al., 2023a;b; Javaheripi et al.,  
029 2023) have demonstrated remarkable capabilities across a variety of tasks. However, their extensive  
030 size often hinders practical deployment. Interest in LLM compression has surged in recent years,  
031 driven by the need to reduce model sizes while maintaining performance (Xiao et al., 2023; Frantar  
032 & Alistarh, 2023; Sun et al., 2023; Zhang et al., 2024b; Malinovskii et al., 2024). This paper focuses  
033 on LLM **post-training pruning** (PTP), a prevalent method for reducing the footprint of pre-trained  
034 weights.

035 A common approach to pruning is magnitude-based pruning, where elements of each layer’s weights  
036 with smaller absolute values are set to zero. In contrast, Wanda (Sun et al., 2023) introduced an in-  
037 novative method that scales the weights by the activations of each layer, demonstrating promising  
038 performance on standard benchmarks. Building upon this, RIA (Zhang et al., 2024b) further im-  
039 proved the approach by evaluating the relative importance of each weight across its corresponding  
040 row and column before pruning. While their empirical results are encouraging, the underlying mech-  
041 anisms remain poorly understood. This leads us to our first question:

042 *Can we provide theoretical support for post-training pruning methods and derive more efficient  
043 algorithms with minimal adaptations to the existing framework?*

044 To deepen our understanding of these popular PTP methods, we introduce a novel formula-  
045 tion—referred to as **Symmetric Weight And Activation** (SymWanda)—that aims to efficiently lever-  
046 age *both* the input activation of a layer and the output for that layer. This symmetric and generalized  
047 approach provides theoretical insights into the mechanisms of established empirical methods such  
048 as Wanda and RIA.

049 Intrinsic PTP methods have demonstrated remarkable performance, as reflected by perplexity scores  
050 and zero-shot accuracy. However, their performance can degrade significantly when the sparsity  
051 ratio is high. This is due to the intrinsic reconstruction error between the pruned weights and the  
052 original pre-trained weights. Minimizing this reconstruction error is particularly important for effi-

054 client post-training pruning. Beyond LLM pruning, we explore further fine-tuning to enhance model  
 055 efficiency and performance. This brings us to our second problem:  
 056

057 *Can we fine-tune pruned LLMs without further training and outperforms state-of-the-art methods  
 058 with minimal effort?*

059 **Dynamic sparse training (DST)** has gained attention for selectively updating and maintaining a  
 060 subset of network parameters throughout the training process while dynamically adapting the sparse  
 061 topology through weight operations. Its proven efficiency in enabling effective training suggests  
 062 DST could be a promising approach for fine-tuning LLMs in an efficient manner. However, DST  
 063 inherently requires backpropagation to train subnetworks, and its effectiveness heavily depends on  
 064 a sufficient number of weight updates (Liu et al., 2021).

065 Interestingly, the pruning-and-growing step within DST offers a training-free methodology, where  
 066 sparse mask adaptation is based solely on weight properties such as magnitude (Mocanu et al.,  
 067 2018). This opens up a potential alternative for addressing the challenge: Instead of relying on  
 068 computationally intensive backpropagation for fine-tuning sparse LLMs, we can explore the iterative  
 069 updating of sparse masks in a training-free manner. Motivated by this insight, we focus on training-  
 070 free fine-tuning approaches.

071 DSnoT (Zhang et al., 2023) introduced a straightforward yet effective method for pruning and growing  
 072 weights using their values and statistical metrics (e.g., expectation and variance) for each ongoing  
 073 pruning row. Inspired by Wanda, DSnoT achieves simplicity but falls short of fully leveraging  
 074 relative weight information, particularly in scenarios where weight distributions are highly non-  
 075 uniform and contain many outliers (Zhang et al., 2024b). To address these limitations, we propose  
 076 incorporating relative weight importance into the growing criterion design. Furthermore, we ob-  
 077 serve that directly optimizing for reconstruction error is suboptimal. To improve performance, we  
 078 introduce a regularization term that relaxes the decision boundary. Our new designs demonstrate  
 079 significant efficiency and consistently achieve promising performance, paving the way for more  
 080 effective and computationally feasible fine-tuning methods for sparse LLMs.

081 Our **contributions** are summarized as follows:

- 082 • We propose a novel formulation, SymWanda, which minimizes the impact of pruning on  
 083 both input activations and output influences of weights. This approach provides theoretical  
 084 insights into the empirical successes of methods such as Wanda and RIA.
- 085 • Building on this formulation, we introduce a series of innovative pruning strategies. Ex-  
 086 tensive experiments validate the effectiveness of our methods. Notably, we incorporate an  
 087 efficient stochastic approach for manipulating relative importance, which achieves superior  
 088 performance with highly reduced sampling cost.
- 089 • We present a novel training-free fine-tuning method  $R^2$ -DSnoT that leverages relative  
 090 weight importance and a regularized decision boundary within a pruning-and-growing  
 091 framework. This approach significantly outperforms strong baselines, achieving remark-  
 092 able results.

## 094 2 RELATED WORK

095 **Traditional model pruning.** Pruning has emerged as a powerful strategy to compress and ac-  
 096 celerate deep neural networks by removing redundant connections while preserving overall perfor-  
 097 mance (Han et al., 2015; Frankle & Carbin, 2018; Hoefler et al., 2021). Early works introduced  
 098 iterative pruning-and-retraining approaches, which iteratively identify unimportant weights, discard  
 099 them, and retrain the resulting sparse network to recover accuracy (LeCun et al., 1989; Han et al.,  
 100 2015). More recent dynamic sparse training techniques (Mocanu et al., 2018; Bellec et al., 2018; Lee  
 101 et al., 2018; Mostafa & Wang, 2019) start from a sparse initialization and continuously prune and  
 102 grow connections throughout training. These methods integrate sparsification into the training loop,  
 103 yielding promising trade-offs between model size and performance. A prominent line of work has  
 104 leveraged learnable thresholds to realize non-uniform sparsity (Kusupati et al., 2020) or combined  
 105 magnitude-based pruning with periodic connectivity updates to regrow valuable weights (Evci et al.,  
 106 2020; Lasby et al., 2023). However, most of these methods still rely on standard back-propagation  
 107 over the full parameter set, which can be prohibitively expensive when scaling up to LLMs.

Table 1: Comparison of LLM post-training pruning algorithms.

Algorithm	W?	Act.?	X	Y	$S_{jk}^{(a)}$	Comment
General Sym.	✓	✓	X	Y	$ \mathbf{W}_{jk}  (\ \mathbf{X}_{:j}\ _2 + \ \mathbf{Y}_{k:}\ _2)$	Lemma 3.1
Marginal	✓	✗	I	0	$ \mathbf{W}_{jk} $	-
Wanda	✓	✓	X	0	$ \mathbf{W}_{jk}  \ \mathbf{X}_{:j}\ _2$	Corollary 3.2
OWanda	✓	✓	0	Y	$ \mathbf{W}_{jk}  \ \mathbf{Y}_{k:}\ _2$	Corollary 3.3
Symmetric	✓	✓	$\mathbf{W}^T$	$\mathbf{W}^T$	$ \mathbf{W}_{jk}  \sqrt{\ \mathbf{W}_{:j}\ _2^2 + \ \mathbf{W}_{:k}\ _2^2}$	Corollary 3.4
RI (v1)	✓	✗	$t_j(1; \dots, 1), t_j = (\sqrt{b} \ \mathbf{W}_{:j}\ _1)^{-1(a)}$	$s_k(1, \dots, 1), s_k = (\sqrt{c} \ \mathbf{W}_{:k}\ _1)^{-1}$	$\ \mathbf{W}_{:j}\ _1^{-1} + \ \mathbf{W}_{:k}\ _1^{-1}$	Theorem 3.5
RI (v2)	✓	✗	$\text{Diag}(\ \mathbf{W}_{:1}\ _1^{-1}, \dots, \ \mathbf{W}_{:b}\ _1^{-1})$	$\text{Diag}(\ \mathbf{W}_{:1}\ _1^{-1}, \dots, \ \mathbf{W}_{:c}\ _1^{-1})$	$\ \mathbf{W}_{:j}\ _1^{-1} + \ \mathbf{W}_{:k}\ _1^{-1}$	Theorem 3.5
RIA	✓	✓	$\delta_{u=j} \delta_{v=p} \mathbf{C}_{:j} \ \mathbf{W}_{:j}\ _1^{-1(c)}$	$\delta_{u=s} \delta_{v=k} \mathbf{C}_{:j} \ \mathbf{W}_{:j}\ _1^{-1}$	$(\ \mathbf{W}_{:j}\ _1^{-1} + \ \mathbf{W}_{:k}\ _1^{-1}) \ \mathbf{X}_{:j}\ _2^{\alpha}$	Lemma 3.6
General (diag.)	✓	✓	$\mathbf{AD}_{\mathbf{X}}^{(d)}$	$\mathbf{D}_{\mathbf{Y}} \mathbf{B}$	$\ \mathbf{A}_{:j}\ _2 \ \mathbf{W}_{:j}\ _1^{-1} + \ \mathbf{B}_{:k}\ _2 \ \mathbf{W}_{:k}\ _1^{-1}$	Lemma 3.7
$\ell_p$ -norm (v1)	✓	✗ <sup>(e)</sup>	$\ \mathbf{W}_{:j}\ _p^{-1} \cdot \ \mathbf{W}_{:j}\ _2^{-1} \cdot \mathbf{W}_{:j}^T$	$\ \mathbf{W}_{:k}\ _p^{-1} \cdot \ \mathbf{W}_{:k}\ _2^{-1} \cdot \mathbf{W}_{:k}^T$	$ \mathbf{W}_{jk}  (\ \mathbf{W}_{:j}\ _p^{-1} + \ \mathbf{W}_{:k}\ _p^{-1})$	Lemma 3.8
$\ell_p$ -norm (v2)	✓	✗	$\ \mathbf{W}_{:j}\ _p^{-1} \cdot \mathbf{u}$	$\ \mathbf{W}_{:k}\ _p^{-1} \cdot \mathbf{v}$	$ \mathbf{W}_{jk}  (\ \mathbf{W}_{:j}\ _p^{-1} + \ \mathbf{W}_{:k}\ _p^{-1})$	Lemma 3.9
StochRIA	✓	✗	$\mathbf{1}_{\{i \in S_j\}} (\ \mathbf{W}_{j:S_j}\ _1 \sqrt{\tau})^{-1}$	$\mathbf{1}_{\{i \in S_k\}} (\ \mathbf{W}_{S_k:k}\ _1 \sqrt{\tau})^{-1}$	$ \mathbf{W}_{jk}  (\ \mathbf{W}_{j:S_j}\ _1^{-1} + \ \mathbf{W}_{S_k:k}\ _1^{-1})$	Lemma 3.10

(a) Without loss of generality, we consider the elimination of a single weight,  $\mathbf{W}_{jk}$ . The detailed explanation can be found in Lemma 3.1 and Section 3.2.

(b) For simplicity, instead of displaying the entire matrices  $\mathbf{X}$  and  $\mathbf{Y}$ , we present the columns  $\mathbf{X}_{:j}$  and the rows  $\mathbf{Y}_{k:}$ . This design is employed in the algorithms RI, RIA,  $\ell_p$ -norm, and StochRIA.

(c) The Kronecker delta, denoted by  $\delta_{ij}$ , is a function of two indices  $i$  and  $j$  that equals 1 if  $i = j$  and 0 otherwise.

(d)  $\mathbf{D}_{\mathbf{X}}$  and  $\mathbf{D}_{\mathbf{Y}}$  are the diagonal matrices associated with  $\mathbf{W}$ , as defined in Section 3.4.

(e) By default, for  $\ell_p$ -norm and StochRIA, we do not consider the input activation. However, the design is similar to the transition from RI to RIA, as described in Section 3.3.

**LLM post-training pruning.** The substantial computational demands of LLMs have raised the development of pruning methods tailored to reduce parameters counts without compromising performance (Li et al., 2023; Zhu et al., 2024). Among these methods, post-training pruning eliminates redundant parameters in a pre-training network without requiring resource-intensive fine-tuning. For instance, SparseGPT (Frantar & Alistarh, 2023) leverages second-order information to solve layer-wise reconstruction problems, supporting both unstructured and N:M structured sparsity (Zhou et al., 2021). Wanda (Sun et al., 2023) introduces a pruning metric that incorporates both weight magnitudes and corresponding input activations, achieving perplexity performance comparable to SparseGPT while surpassing simple magnitude-based pruning. The RIA method (Zhang et al., 2024b) builds on Wanda by considering relative weight importance, offering performance improvements at minimal additional cost. Moreover, DSnoT (Zhang et al., 2023) proposes pruning and regrowing weights based on statistical properties (e.g., mean and variance) in each pruning row, obviating the need for retraining.

### 3 SYMMETRIC WANDA

#### 3.1 PREREQUISITES

Post-training pruning is defined as follows: consider a target sparsity ratio  $\varepsilon \in [0, 1]$ , a set of calibration inputs  $\mathbf{X} \in \mathbb{R}^{a \times b}$ , and pre-trained weights  $\mathbf{W} \in \mathbb{R}^{b \times c}$ . For clarity in the mathematical framework, we abstract the dimensions of inputs and weights. Specifically, in the context of large language models, let  $a := C_{\text{in}}$ ,  $b := N \times L$ , and  $c \equiv C_{\text{out}}$ , where  $N$  and  $L$  denote the batch size and sequence length, respectively. The objective is to identify an optimal pruned weight matrix  $\widetilde{\mathbf{W}} \in \mathbb{R}^{b \times c}$  that minimizes:

$$f(\widetilde{\mathbf{W}}) := \|\mathbf{X}(\widetilde{\mathbf{W}} - \mathbf{W})\|_F^2, \quad (\text{InpRecon})$$

where the optimization challenge is:

$$\text{minimize } f(\widetilde{\mathbf{W}}) \text{ s.t. } \text{Mem}(\widetilde{\mathbf{W}}) \leq (1 - \varepsilon) \text{Mem}(\mathbf{W}),$$

where  $\text{Mem}(\cdot)$  denotes the memory consumption associated with a weight matrix, and (InpRecon) quantifies the input reconstruction error.

This formulation applies to various post-training compression techniques, including both pruning (Frantar & Alistarh, 2023; Sun et al., 2023; Zhang et al., 2024b) and quantization (Frantar et al., 2023; Egiazarian et al., 2024). Our focus here is specifically on post-training pruning.

162 3.2 SYMMETRIC WANDA: NEW FORMULATIONS  
163

164 Building upon the methods introduced in Wanda (Sun et al., 2023), which considered both weights  
165 and activations, and later improvements by RIA (Zhang et al., 2024b), which analyzed the relative  
166 importance of weights by summing over corresponding rows and columns, we provide new insights  
167 by redefining our optimization objective. Apart from the previous defined input calibration  $\mathbf{X}$ , we  
168 particularly introduce the output calibration  $\mathbf{Y} \in \mathbb{R}^{c \times d}$ . Considering both the input and output  
169 dependencies, we express the objective as:

$$170 \quad 171 \quad g(\widetilde{\mathbf{W}}) := \|\mathbf{X}(\widetilde{\mathbf{W}} - \mathbf{W})\|_F + \|(\widetilde{\mathbf{W}} - \mathbf{W})\mathbf{Y}\|_F, \quad (Sym)$$

172 and propose to solve:

$$174 \quad 175 \quad \text{minimize } g(\widetilde{\mathbf{W}}), \text{ s.t. } \text{Mem}(\widetilde{\mathbf{W}}) \leq (1 - \varepsilon)\text{Mem}(\mathbf{W}).$$

176 We refer to the method that utilizes the general matrix in (Sym) without instantiation as SymWanda,  
177 which is designed to minimize the reconstruction error affected by both the input  $\mathbf{X}$  and the output  
178  $\mathbf{Y}$ . It is important to note that this formulation employs *non-squared* Frobenius norms to facilitate  
179 better theoretical interpretations. A squared norm version is also provided in Appendix B for com-  
180 parison. We elucidate the efficacy of both approaches and provide new theoretical insights into the  
181 performance advantages previously observed with Wanda and RIA.

182 **Lemma 3.1.** *Assume we aim to eliminate a single weight  $\mathbf{W}_{jk}$ , setting  $\widetilde{\mathbf{W}}_{jk} = 0$  and keeping all  
183 other weights unchanged. The simplified expression for  $g(\widetilde{\mathbf{W}})$  becomes:*

$$186 \quad 187 \quad g(\widetilde{\mathbf{W}}) = |\mathbf{W}_{jk}| (\|\mathbf{X}_{:j}\|_2 + \|\mathbf{Y}_{k:}\|_2) := \mathbf{S}_{jk}, \quad (1)$$

188 where  $\mathbf{X}_{:j}$  and  $\mathbf{Y}_{k:}$  represent the  $j$ -th column and  $k$ -th row of  $\mathbf{X}$  and  $\mathbf{Y}$ , respectively.

189 This formulation (1) underscores the impact of individual weights on the error metrics and guides  
190 the pruning process. While Lemma 3.1 simplifies the formulation for pruning a single weight, the  
191 general approach can be extended to multiple weights iteratively. This method facilitates a robust  
192 pruning strategy that is backed by both empirical results and theoretical foundations, bridging the  
193 gap in understanding observed in prior studies such as Wanda (Sun et al., 2023) and RIA (Zhang  
194 et al., 2024b).

195 **Corollary 3.2.** *Setting  $\mathbf{Y} = \mathbf{0} \in \mathbb{R}^{c \times d}$  transitions our method to input Wanda, described by  $\mathbf{S}_{jk} :=$   
196  $|\mathbf{W}_{jk}| \|\mathbf{X}_{:j}\|_2$ .*

197 This directly aligns with the objective in Sun et al. (2023), demonstrating that Wanda is a specific  
198 case under our broader framework.

200 **Corollary 3.3.** *Conversely, choosing  $\mathbf{X} = \mathbf{0} \in \mathbb{R}^{a \times b}$  simplifies our pruning method to what we  
201 term output Wanda (denoted as OWanda), where the score matrix becomes  $\mathbf{S}_{jk} := |\mathbf{W}_{jk}| \|\mathbf{Y}_{k:}\|_2$ .*

202 **Corollary 3.4.** *By setting  $\mathbf{X} = \mathbf{W}^\top \in \mathbb{R}^{c \times b}$  ( $a = c$ ) and  $\mathbf{Y} = \mathbf{W}^\top \in \mathbb{R}^{c \times b}$  ( $d = b$ ), the score  
203 matrix  $\mathbf{S}_{jk}$  is redefined as  $|\mathbf{W}_{jk}| (\|\mathbf{W}_{:j}\|_2 + \|\mathbf{W}_{:k}\|_2)$ .*

205 This configuration suggests an alternative masking approach and segues into a further analysis on  
206 how our method encompasses both Wanda and RIA as special cases. The following theorem provides  
207 a provable construction to recover the relative importance design in Zhang et al. (2024b).

208 **Theorem 3.5.** *Assuming  $a = b$  and  $c = d$ , consider one of the following strategies:*

- 210 •  $\mathbf{X}_{:j} := t_j(1; \dots; 1) \in \mathbb{R}^{b \times 1}$  and  $\mathbf{Y}_{k:} := s_k(1, \dots, 1) \in \mathbb{R}^{1 \times c}$ , where  $t_j = (\sqrt{b} \|\mathbf{W}_{:j}\|_1)^{-1}$   
211 and  $s_k = (\sqrt{c} \|\mathbf{W}_{:k}\|_1)^{-1}$ .
- 212 •  $\mathbf{X} = \text{Diag}(\|\mathbf{W}_{1:}\|_1^{-1}, \dots, \|\mathbf{W}_{b:}\|_1^{-1})$  and  $\mathbf{Y} = \text{Diag}(\|\mathbf{W}_{:1}\|_1^{-1}, \dots, \|\mathbf{W}_{:c}\|_1^{-1})$ .

213 For these configurations, the condition  $\|\mathbf{X}_{:j}\|_2 + \|\mathbf{Y}_{k:}\|_2 = \alpha_{jk} := \|\mathbf{W}_{:j}\|_1^{-1} + \|\mathbf{W}_{:k}\|_1^{-1}$  holds  
214 for all  $j, k$ .

This theorem elucidates that our methodology can invariably reconstruct the framework of relative importance RI in (Zhang et al., 2024b), validating the adaptability and breadth of our proposed pruning strategy.

### 3.3 FROM RELATIVE IMPORTANCE (RI) TO RI ACTIVATION

In Theorem 3.5, we revisit the concept of Relative Importance (RI). Specifically, we represent RI by the following equation:

$$S_{jk} = \|\mathbf{W}_{jk}\| \|\mathbf{W}_{j:}\|_1^{-1} + \|\mathbf{W}_{jk}\| \|\mathbf{W}_{:k}\|_1^{-1} := RI_{jk}.$$

Zhang et al. (2024b) also introduces an enhanced version of RI, termed RI with Activation (RIA), which incorporates the  $\ell_2$ -norm of activations:

$$RIA_{jk} = RI_{jk} \cdot \|\mathbf{X}_{:j}\|_2^\alpha, \quad (2)$$

where  $\alpha$  is controlling the strength of activations.

This section aims to explore the derivation of RIA with theoretical grounding in RI. To clarify our notation and avoid confusion, we are aiming at finding the suitable  $\mathbf{A} \in \mathbb{R}^{a \times b}$  and  $\mathbf{B} \in \mathbb{R}^{c \times d}$  such as:

$$\|\mathbf{A}_{j:}\|_2 + \|\mathbf{B}_{:k}\|_2 = \left( \|\mathbf{W}_{j:}\|_1^{-1} + \|\mathbf{W}_{:k}\|_1^{-1} \right) \cdot \|\mathbf{C}_{:j}\|_2^\alpha,$$

where  $\mathbf{C}_{:j}$  will be instantiated as  $\mathbf{X}_{:j}$  to satisfy Equation (2).

**Lemma 3.6.** *Let  $p$  be a valid column index for  $\mathbf{A}$ . Define  $\mathbf{A}_{uv} = 0$  for all  $(u, v) \neq (j, p)$ , and  $\mathbf{A}_{j,p} = \|\mathbf{C}_{:j}\|_2^\alpha \|\mathbf{W}_{j:}\|_1^{-1}$ . Similarly, let  $s$  be a valid row index for  $\mathbf{B}$ . Define  $\mathbf{B}_{uv} = 0$  for all  $(u, v) \neq (s, k)$ , and  $\mathbf{B}_{s,k} = \|\mathbf{C}_{:j}\|_2^\alpha \|\mathbf{W}_{:k}\|_1^{-1}$ . Then we recover Equation (2).*

The nonzero element in  $\mathbf{A}$  ensures that the  $\ell_2$ -norm of the  $j$ -th row of  $\mathbf{A}$  is:  $\|\mathbf{A}_{j:}\|_2 = \|\mathbf{W}_{j:}\|_1^{-1} \cdot \|\mathbf{C}_{:j}\|_2^\alpha$ . Similarly, the nonzero element in  $\mathbf{B}$  ensures that the  $\ell_2$ -norm of the  $k$ -th column of  $\mathbf{B}$  is:  $\|\mathbf{B}_{:k}\|_2 = \|\mathbf{W}_{:k}\|_1^{-1} \cdot \|\mathbf{C}_{:j}\|_2^\alpha$ . Combining these norms fulfills the intended equation.

### 3.4 GENERAL SOLUTION

In Theorem 3.5, we presented two distinct strategies for recovering the relative importance as described in Zhang et al. (2024b). Following this, in Lemma 3.6, we constructed a method that accounts for both the weights and the input activations. Inspired by the diagonal design in Theorem 3.5, we now propose a general variant that considers both the weights and the activations.

Given that  $\mathbf{D}_X \in \mathbb{R}^{b \times b}$  and  $\mathbf{D}_Y \in \mathbb{R}^{c \times c}$  are diagonal matrices with entries defined as  $(\mathbf{D}_X)_{ii} = x_i = \|\mathbf{W}_{i:}\|_1^{-1}$  and  $(\mathbf{D}_Y)_{ii} = y_i = \|\mathbf{W}_{:i}\|_1^{-1}$  respectively, and  $\mathbf{A} \in \mathbb{R}^{a \times b}$  and  $\mathbf{B} \in \mathbb{R}^{c \times d}$  are arbitrary matrices, our objective is to compute the sum of norms:  $\|(\mathbf{AD}_X)_{:j}\|_2 + \|(\mathbf{D}_Y \mathbf{B})_{k:}\|_2$ .

**Lemma 3.7.** *Given the above definition, we show*

$$\|(\mathbf{AD}_X)_{:j}\|_2 + \|(\mathbf{D}_Y \mathbf{B})_{k:}\|_2 = \frac{\|\mathbf{A}_{:j}\|_2}{\|\mathbf{W}_{j:}\|_1} + \frac{\|\mathbf{B}_{k:}\|_2}{\|\mathbf{W}_{:k}\|_1}.$$

The utilization of the diagonal matrices  $\mathbf{D}_X$  and  $\mathbf{D}_Y$  simplifies the sum of the norms to the expressions derived above, offering insights into the influence of the weight matrix  $\mathbf{W}$  on the norms of matrix transformations.

### 3.5 ENHANCED RELATIVE IMPORTANCE STRATEGIES

Beyond RIA, we propose several alternative strategies for relative importance that aim to minimize  $S_{jk}$  in Equation (1).

270 3.5.1 GENERALIZED  $\ell_p$ -NORM  
271

272 Expanding beyond the conventional  $\ell_1$ -norm, we explore the utility of the  $\ell_p$ -norm in designing  
273 score matrices. In our approach, mirroring the strategy outlined in Theorem 3.5 for reconstructing  
274 RIA outcomes, we define the score as:

$$276 \quad \mathbf{S}_{jk} = |\mathbf{W}_{jk}|(\|\mathbf{W}_{j:}\|_p^{-1} + \|\mathbf{W}_{:k}\|_p^{-1}). \quad (3)$$

278 Next, we are interested in finding the explicit formulation of  $\mathbf{X}$  and  $\mathbf{Y}$  instead of the norm represen-  
279 tation when constructing the general  $\ell_p$ -norm.

280 **Lemma 3.8** (Generalized  $\ell_p$ -norm). *Let  $\mathbf{X}_{:j} = \|\mathbf{W}_{j:}\|_p^{-1} \cdot \|\mathbf{W}_{j:}\|_2^{-1} \cdot \mathbf{W}_{j:}^\top$  and  $\mathbf{Y}_{k:} =$   
281  $\|\mathbf{W}_{:k}\|_p^{-1} \cdot \|\mathbf{W}_{:k}\|_2^{-1} \cdot \mathbf{W}_{:k}^\top$ , we recover Equation (3).*

283 Since the equation only requires  $\|\mathbf{X}_{:j}\|_2 = \|\mathbf{W}_{j:}\|_p^{-1}$ , any vector with this  $\ell_2$ -norm will satisfy the  
284 condition. Inspired by this fact, we can consider the random unit vector scaling in the below lemma.

285 **Lemma 3.9** (Random unit vector scaling). *Choose any unit vector  $\mathbf{u}, \mathbf{v}$  (i.e.,  $\|\mathbf{u}\|_2 = 1, \|\mathbf{v}\|_2 = 1$ )  
286 and set  $\mathbf{X}_{:j} = \|\mathbf{W}_{j:}\|_p^{-1} \cdot \mathbf{u}$  and  $\mathbf{Y}_{k:} = \|\mathbf{W}_{:k}\|_p^{-1} \cdot \mathbf{v}$  ensuring Equation (3).*

288 3.5.2 STOCHASTIC RELATIVE IMPORTANCE  
289

290 Considering the computational and noise challenges associated with summing all elements across  
291 the full rows and columns of large matrices, we introduce a stochastic approach that involves sam-  
292 pling a subset of each row and column. This method assesses the effects of varying subset sizes,  
293 denoted by  $\tau$ , where  $\tau < \min(b, c)$ , on the overall performance. Specifically, we aim to:

294 a) Evaluate the sensitivity of the final performance to the size of  $\tau$  when  $\tau$  is reasonably large.  
295 b) Determine if random sampling can enhance the results compared to a deterministic approach.

297 For this, we define the score matrix for a randomly sampled subset as:

$$298 \quad \mathbf{S}_{jk} = |\mathbf{W}_{jk}|(\|\mathbf{W}_{j:S_j}\|_1^{-1} + \|\mathbf{W}_{S_k:k}\|_1^{-1}), \quad (4)$$

300 where  $S_j$  and  $S_k$  represent the sampled indices from the  $j$ -th row and  $k$ -th column, respectively,  
301 each with a cardinality of  $\tau$ . This approach builds on the RIA-inspired framework, adapting it for  
302 practical scenarios involving large-scale data.

303 For RIA in each weight layer, the reweighting sampling complexity is  $O(b + c)$ . In LLMs,  $b$  and  $c$   
304 are always very large. Let's say the selection ratio is  $\beta$ , then for the stochastic relative importance  
305 design, the sampling complexity can be reduced to  $O(\beta \min(b, c))$ , which has been highly reduced.

307 **Lemma 3.10.** *Let  $S_j$  and  $S_k$  be index sets, and let  $\tau > 0$ . Define the vectors  $\mathbf{X}_{:j}$  and  $\mathbf{Y}_{k:}$  by*

$$308 \quad \mathbf{X}_{:j}(i) = \frac{\mathbf{1}_{\{i \in S_j\}}}{\|\mathbf{W}_{j:S_j}\|_1 \sqrt{\tau}}, \quad \mathbf{Y}_{k:}(i) = \frac{\mathbf{1}_{\{i \in S_k\}}}{\|\mathbf{W}_{S_k:k}\|_1 \sqrt{\tau}}.$$

310 *Then these vectors satisfy Equation (4).*

312 3.6 TRAINING-FREE FINE-TUNING  
313

314 We explore training-free fine-tuning within the context of the pruning-and-growing framework.  
315 Specifically, for the pruned weight matrix  $\widetilde{\mathbf{W}}$ , we aim to minimize the reconstruction error as de-  
316 fined in (Sym). Initially, we identify the growth index, followed by the pruning index, to maintain  
317 a consistent sparsity ratio. DSnoT (Zhang et al., 2023) developed a growing criterion based on the  
318 expected change in reconstruction error when reinstating a weight. Particularly, for any given weight  
319 row  $q \in [1, b]$ , the index  $i$  is determined as follows:

$$320 \quad i = \arg \max_r \text{sign}(\mathbb{E}[\epsilon_q]) \cdot \widetilde{\mathbf{W}}_{q,r} \cdot \mathbb{E}[\mathbf{X}_q] / \text{Var}(\mathbf{X}_q),$$

322 where  $\epsilon_q := \mathbf{W}_{q:} \mathbf{X} - \widetilde{\mathbf{W}}_{q:} \mathbf{X}$  denotes the reconstruction error of the  $q$ -th row across different input  
323 activations. It is important to note that for simplicity, output activations are not considered here,

which may provide an interesting avenue for future exploration. The functions  $\text{sign}(\cdot)$ ,  $\mathbb{E}[\cdot]$ , and  $\text{Var}(\cdot)$  denote the standard sign function, expectation, and variance of given inputs over  $N \times L$  tokens, respectively. Drawing inspiration from the Wanda metric, the DSnoT model defines the pruning index  $j$  as:

$$j = \arg \min_{r: \Delta(q, r) < 0} |\widetilde{\mathbf{W}}_{q, r}| \|\mathbf{X}_q\|_2,$$

where  $\Delta(q, r) := \text{sign}(\mathbb{E}[\epsilon_q]) (\widetilde{\mathbf{W}}_{q, r} \cdot \mathbb{E}[\mathbf{X}_q])$ .

Several simple yet effective modifications have been incorporated into the pruning-and-growing framework:

**a) Relative weight importance.** Both in determining the growing index  $i$  and the pruning index  $j$ , we incorporate global information, emphasizing the relative importance of weights in neuron selection.

**b) Square root activation.** Our follow-up experiments on Wanda and RIA demonstrate the benefits of square root activation in determining the pruning index  $j$ .

**c) Regularized objective.** The method MagR (Zhang et al., 2024a) found that adding an  $\ell_\infty$  norm helps reduce the magnitude of weights during quantization. Here, we adopt a more general regularizer, considering a general  $\ell_p$  norm and focusing on specific rows rather than entire layers to reduce communication costs.

Define  $\mathbf{D}_{q, r} := \|\widetilde{\mathbf{W}}_{q, r}\|_1^{-1} + \|\widetilde{\mathbf{W}}_{q, r}\|_1^{-1}$ . The updated rule for identifying the growing index  $i$  is formalized as:

$$i = \arg \max_r \left\{ \text{sign}(\mathbb{E}[\epsilon_q]) \cdot \mathbf{D}_{q, r} \cdot \frac{\mathbb{E}[\mathbf{X}_q]}{\text{Var}(\mathbf{X}_q)} + \gamma_1 \|\widetilde{\mathbf{W}}_q\|_p \right\}, \quad (5)$$

where  $\gamma_1$  is the growing regularization parameter, striking a balance between fidelity and the  $\ell_p$  regularizer. Similarly, the pruning index  $j$  is now defined as:

$$j = \arg \min_{r: \Delta(q, r) < 0} \left\{ |\widetilde{\mathbf{W}}_{q, r}| \cdot \mathbf{D}_{q, r} \cdot \|\mathbf{X}_q\|_2^\alpha + \gamma_2 \|\widetilde{\mathbf{W}}_q\|_p \right\}, \quad (6)$$

where  $\Delta(q, r) := \text{sign}!(\mathbb{E}[\epsilon_q]) (\widetilde{\mathbf{W}}_{q, r} \cdot \mathbf{D}_{q, r} \cdot \mathbb{E}[\mathbf{X}_q])$ , and  $\gamma_2$  denotes the pruning regularization parameter.

We name this approach *Relative and Regularized Dynamic Sparse No Training* ( $R^2$ -DSnoT). It enables efficient network fine-tuning without additional training, conserving computational resources while enhancing performance.

## 4 EXPERIMENTS

**Setup and configurations.** We assess the proposed methods across a broad spectrum of popular LLMs, including LlaMA2 (7b-13b) (Touvron et al., 2023b), LlaMA3-8b (Dubey et al., 2024), OPT-1.3b (Zhang et al., 2022a). We utilize publicly available model checkpoints from the HuggingFace Transformers library (Wolf et al., 2020) for our evaluations. Each experiment, focused on post-training pruning, is conducted on an NVIDIA A100-80G GPU. The effectiveness of each pruned model is primarily measured using the perplexity score on the WikiText-2 dataset (Merity et al., 2016). For calibration, we use 128 samples from the C4 dataset (Raffel et al., 2020), with each sample comprising 2048 tokens. This approach ensures consistency with the settings used in baseline methods, enabling a fair comparison.

### 4.1 EFFICIENCY OF STOCHASTIC METHODS

We begin by examining two key designs discussed in Section 3.5: the generalized  $\ell_p$  norm and stochastic relative importance. The results for the  $\ell_p$  norm are presented in Appendix D.2, where we confirm that  $p = 1$  is indeed optimal. We also compare various  $\ell_p$  norm reweighting strategies,

378  
379  
380  
381  
382  
383  
384  
385  
386  
387  
388  
389  
390  
391  
392  
393  
394  
395  
396  
397  
398  
399  
400  
401  
402  
403  
404  
405  
406  
407  
408  
409  
410  
411  
412  
413  
414  
415  
416  
417  
418  
419  
420  
421  
422  
423  
424  
425  
426  
427  
428  
429  
430  
431

Table 2: Perplexity comparison between StochRIA ( $\beta=0.1$ ) and RIA on Wikitext-2 with  $\alpha=1$ . Mean  $\pm$  std over 5 trials is shown for StochRIA; differences from RIA are in blue (better) and red (worse).

Sparsity	Method	Sampling	LlaMA2-7b	LlaMA2-13b	LlaMA3-8b	OPT-1.3b
-	Dense	-	5.47	4.88	6.14	14.62
50%	Magnitude	-	16.03	6.83	205.44	1712.39
	Wanda	-	7.79	6.28	10.81	22.19
	RIA	Full	6.88	5.95	9.44	18.94
2:4	stochRIA	10%	6.91 <sup>±0.032</sup> <sub>−0.03</sub>	5.95 <sup>±0.033</sup> <sub>±0</sub>	9.46 <sup>±0.025</sup> <sub>−0.02</sub>	18.78 <sup>±0.050</sup> <sub>±0.16</sub>
	RIA	Full	11.31	8.40	22.89	27.43
4:8	stochRIA	10%	11.41 <sup>±0.046</sup> <sub>−0.04</sub>	8.44 <sup>±0.016</sup> <sub>±0.15</sub>	23.74 <sup>±0.230</sup> <sub>±0.15</sub>	26.78 <sup>±0.127</sup> <sub>±0.65</sub>
	RIA	Full	8.39	6.74	13.77	21.59
10:16	stochRIA	10%	8.44 <sup>±0.014</sup> <sub>−0.05</sub>	6.74 <sup>±0.013</sup> <sub>±0</sub>	13.93 <sup>±0.095</sup> <sub>−0.16</sub>	21.49 <sup>±0.089</sup> <sub>±0.10</sub>

Table 3: Perplexity scores on Wikitext-2 after training-free fine-tuning. The sparsity ratio is set to 60% and  $\alpha = 0.5$ .

Base	FT	LlaMA2-7b	LlaMA2-13b	LlaMA3-8b
Dense	-	5.47	4.88	6.14
Magnitude	-	6.9e3	10.10	4.05e5
Magnitude	DSnoT	4.1e3	10.19	4.18e4
Magnitude	$R^2$ -DSnoT	<b>2.4e2</b>	<b>10.09</b>	<b>1.44e4</b>
Wanda	-	<b>9.72</b>	7.75	21.36
Wanda	DSnoT	10.23	<b>7.69</b>	20.70
Wanda	$R^2$ -DSnoT	10.08	<b>7.69</b>	<b>20.50</b>
RIA	-	10.29	7.85	21.09
RIA	DSnoT	9.97	7.82	19.51
RIA	$R^2$ -DSnoT	<b>9.96</b>	<b>7.78</b>	<b>18.99</b>

with the results presented in Appendix D.3. Our primary focus, however, is on the findings related to stochastic relative importance, which, to the best of our knowledge, represents the first approach to incorporating stochasticity into LLM post-training pruning.

We analyze the impact of stochastic relative importance, with the results summarized in Table 2. The stochRIA results correspond to a sampling ratio of  $\beta = 0.1$ . Each reported value represents the mean performance across five trials with different random seeds. Notably, even with less than only 10% of the samples used to estimate relative importance, the results remain sufficiently representative, leading to promising outcomes.

In addition to unstructured pruning with a sparsity ratio of 0.5, we also explore structured pruning using the N:M pattern (Zhou et al., 2021; Zhang et al., 2022b). The results are presented in Table 2. Noticed that here for intuitive comparison between RIA and stochRIA, we use the plain N:M structural pruning without channel permutation. These results consistently demonstrate the benefits and efficiency of our proposed method, stochRIA.

Furthermore, when aggregating results across all examined models and baselines, stochRIA achieves an accumulated perplexity that is 0.66 lower than RIA, demonstrating the effectiveness of a stochastic design. This stochastic sampling preserves the diversity needed to handle subpopulations that rely on lower-average-importance weights while also helping preserve generalization by avoiding the dilution of salient features.

We also evaluate the performance across different sampling ratios, as shown in Appendix D.4. Our main takeaway is that stochRIA exhibits stable and competitive performance relative to RIA, particularly when the sampling ratio  $\tau \geq 0.05$ . At or above this threshold, the performance remains robust and occasionally surpasses less noisy sampling configurations. However, at an extremely low sampling ratio of  $\tau = 0.01$ , a significant performance drop is observed. Consequently, we adopt  $\tau = 0.1$  as the default setting for our experiments.

## 4.2 TRAINING-FREE FINE-TUNING COMPARISONS

The intrinsic gap between pruned weights and the original, unpruned pretrained weights underscores the importance of minimizing reconstruction loss to achieve promising results. We introduced  $R^2$ -DSnoT, which incorporates relative weight reweighting and a regularized decision boundary during the dynamic sparse refinement step, all without additional training. Perplexity scores, as shown in Table 3, reveal that our  $R^2$ -DSnoT approach consistently surpasses baseline methods and the previous state-of-the-art DSnoT without fine-tuning. For instance, Magnitude exhibited subpar perplexity scores on LlaMA2-7b and LlaMA3-8b; however, our  $R^2$ -DSnoT achieved perplexity reductions of 96.5% and 96.4%, respectively. These results not only validate  $R^2$ -DSnoT’s efficacy but also offer guidance for scenarios involving high sparsity or underperforming pruned models, with minimal effort and no additional training.

**Zero-shot performance.** To provide a comprehensive evaluation, we also conducted zero-shot classification tests using seven well-regarded datasets. These tests assess the pruned models’ ability to accurately categorize objects or data points into previously unseen categories. We employed

432 Table 4: Accuracies (%) for LLaMA2 models on 7 zero-shot tasks at 60% unstructured sparsity.  
433

434 Params	435 Method	436 BoolQ	437 RTE	438 HellaSwag	439 WinoGrande	440 ARC-e	441 ARC-c	442 OBQA	443 Mean
444 LlaMA2-7b	Dense	77.7	62.8	57.2	69.2	76.4	43.4	31.4	57.9
	Magnitude	41.2	51.3	37.0	55.7	50.0	27.0	16.2	39.3
	w. DSnoT	43.2	54.2	38.4	56.4	53.3	27.7	20.6	41.1
	w. $R^2$ -DSnoT	50.9	52.0	39.8	56.8	56.6	28.3	23.4	43.4
	RIA	66.1	53.1	43.5	63.2	64.6	30.2	26.0	49.5
	w. DSnoT	65.5	53.4	44.7	64.6	65.3	31.7	26.4	50.2
	w. $R^2$ -DSnoT	65.2	53.8	44.7	65.1	65.0	31.6	27.0	50.3
	Dense	81.3	69.7	60.1	73.0	80.1	50.4	34.8	64.2
	Magnitude	37.8	52.7	30.7	51.0	39.7	23.4	14.4	35.7
445 LlaMA3-8b	w. DSnoT	37.8	52.7	33.4	49.9	43.5	23.0	14.8	36.4
	w. $R^2$ -DSnoT	37.8	52.7	33.1	52.1	43.9	23.6	14.8	37.1
	RIA	70.2	53.4	39.7	61.7	61.1	28.6	20.4	47.9
446	w. DSnoT	70.7	53.4	40.3	61.3	61.7	28.0	20.0	47.9
	w. $R^2$ -DSnoT	70.4	53.4	40.3	61.9	61.2	28.3	21.0	48.1

447  
448 the methodology described by Sun et al. (2023) and utilized tasks from the EleutherAI LM Harness  
449 (Gao et al., 2021), including BoolQ (Clark et al., 2019), RTE (Wang et al., 2018), HellaSwag (Zellers  
450 et al., 2019), WinoGrande (Sakaguchi et al., 2021), ARC (Easy and Challenge) (Clark et al., 2018),  
451 and OpenbookQA (Mihaylov et al., 2018). The results, presented in Table 4, show that  $R^2$ -DSnoT  
452 consistently outperforms DSnoT in zero-shot tasks, confirming its effectiveness. To the best of our  
453 knowledge,  $R^2$ -DSnoT establishes a new state-of-the-art for training-free pruning and fine-tuning  
454 methods in zero-shot performance.

## 456 5 DISCUSSION, LIMITATIONS, AND FUTURE WORK

457 This work introduced a unified symmetric formulation for LLM pruning, offering theoretical in-  
458 sight and strong empirical performance. Building on these findings, we outline several promising  
459 directions for future research:

460 **Beyond pruning.** Our exploration of Wanda and RIA introduced the symmetric objective in (Sym),  
461 initially aimed at post-training pruning for LLMs. However, our approach is extendable to post-  
462 training quantization and training-aware compression (Frantar et al., 2023; Egiazarian et al., 2024;  
463 Malinovskii et al., 2024), making these areas promising for future research.

464 **Better sampling.** In Section 4.1, we demonstrated that selective sampling of matrix rows and  
465 columns enhances both performance and efficiency by maintaining diversity in lower-importance  
466 weights. Future research could explore asymmetric or non-uniform sampling within the (Sym)  
467 framework to further optimize performance.

468 **Exploring symmetric designs.** As shown in Table 1, general and diagonal-specific symmetric  
469 designs for LLM compression highlight the potential of symmetric weight and activation patterns.  
470 Extending these approaches to distributed and federated settings (Yi et al., 2024; Ye et al., 2024)  
471 could also be valuable.

## 472 6 CONCLUSION

473 This study systematically analyzed post-training pruning methods, particularly Wanda and RIA, and  
474 provided both empirical evidence and theoretical insights into the role of input activations and rel-  
475 ative weight importance, formalized through a unified symmetric objective in (Sym) that connects  
476 pruning with broader compression techniques. Building on this foundation, we proposed stochRIA,  
477 a stochastic variant that improves efficiency via selective sampling without compromising accuracy,  
478 and validated its effectiveness across various sparsity levels and model architectures. We further  
479 introduced a lightweight, training-free fine-tuning step within a prune-and-grow framework, achiev-  
480 ing consistent improvements in perplexity and classification tasks over existing baselines. Together,  
481 these contributions advance both the theoretical understanding and practical utility of post-training  
482 pruning, and open up future directions in training-aware compression, quantization, and personal-  
483 alized deployment of large language models.

486 REFERENCES  
487

488 Guillaume Bellec, David Kappel, Wolfgang Maass, and Robert Legenstein. Deep rewiring: Training  
489 very sparse deep networks. In *International Conference on Learning Representations*, 2018.

490 Christopher Clark, Kenton Lee, Ming-Wei Chang, Tom Kwiatkowski, Michael Collins, and Kristina  
491 Toutanova. Boolq: Exploring the surprising difficulty of natural yes/no questions. *arXiv preprint*  
492 *arXiv:1905.10044*, 2019.

493 Peter Clark, Isaac Cowhey, Oren Etzioni, Tushar Khot, Ashish Sabharwal, Carissa Schoenick, and  
494 Oyvind Tafjord. Think you have solved question answering? try arc, the ai2 reasoning challenge.  
495 *arXiv preprint arXiv:1803.05457*, 2018.

496 Abhimanyu Dubey, Abhinav Jauhri, Abhinav Pandey, Abhishek Kadian, Ahmad Al-Dahle, Aiesha  
497 Letman, Akhil Mathur, Alan Schelten, Amy Yang, Angela Fan, et al. The llama 3 herd of models.  
498 *arXiv preprint arXiv:2407.21783*, 2024.

499 500 Vage Egiazarian, Andrei Panferov, Denis Kuznedelev, Elias Frantar, Artem Babenko, and Dan Al-  
501 istarh. Extreme compression of large language models via additive quantization. In *Forty-first*  
502 *International Conference on Machine Learning*, 2024.

503 504 Utku Evci, Trevor Gale, Jacob Menick, Pablo Samuel Castro, and Erich Elsen. Rigging the lottery:  
505 Making all tickets winners. In *International conference on machine learning*, pp. 2943–2952.  
506 PMLR, 2020.

507 508 Jonathan Frankle and Michael Carbin. The lottery ticket hypothesis: Finding sparse, trainable neural  
509 networks. In *International Conference on Learning Representations*, 2018.

510 511 Elias Frantar and Dan Alistarh. Sparsegpt: Massive language models can be accurately pruned in  
512 one-shot. In *International Conference on Machine Learning*, pp. 10323–10337. PMLR, 2023.

513 514 Elias Frantar, Saleh Ashkboos, Torsten Hoefler, and Dan Alistarh. OPTQ: Accurate quantization  
515 for generative pre-trained transformers. In *The Eleventh International Conference on Learning*  
516 *Representations*, 2023. URL <https://openreview.net/forum?id=tcbBPnfwxS>.

517 518 Leo Gao, Jonathan Tow, Stella Biderman, Sid Black, Anthony DiPofi, Charles Foster, Laurence  
519 Golding, Jeffrey Hsu, Kyle McDonell, Niklas Muennighoff, et al. A framework for few-shot  
language model evaluation. *Version v0. 0.1. Sept*, 10:8–9, 2021.

520 521 Song Han, Jeff Pool, John Tran, and William Dally. Learning both weights and connections for  
522 efficient neural network. *Advances in neural information processing systems*, 28, 2015.

523 524 Torsten Hoefler, Dan Alistarh, Tal Ben-Nun, Nikoli Dryden, and Alexandra Peste. Sparsity in deep  
525 learning: Pruning and growth for efficient inference and training in neural networks. *Journal of*  
*Machine Learning Research*, 22(241):1–124, 2021.

526 527 Mojan Javaheripi, Sébastien Bubeck, Marah Abdin, Jyoti Aneja, Sébastien Bubeck, Caio  
528 César Teodoro Mendes, Weizhu Chen, Allie Del Giorno, Ronen Eldan, Sivakanth Gopi, et al.  
529 Phi-2: The surprising power of small language models. *Microsoft Research Blog*, 2023.

530 531 Aditya Kusupati, Vivek Ramanujan, Raghav Somani, Mitchell Wortsman, Prateek Jain, Sham  
532 Kakade, and Ali Farhadi. Soft threshold weight reparameterization for learnable sparsity. In  
533 *International Conference on Machine Learning*, pp. 5544–5555. PMLR, 2020.

534 535 Mike Lasby, Anna Golubeva, Utku Evci, Mihai Nica, and Yani Ioannou. Dynamic sparse training  
536 with structured sparsity. *arXiv preprint arXiv:2305.02299*, 2023.

537 538 Yann LeCun, John Denker, and Sara Solla. Optimal brain damage. *Advances in neural information*  
*processing systems*, 2, 1989.

539 Namhoon Lee, Thalaiyasingam Ajanthan, and Philip HS Torr. Snip: Single-shot network pruning  
based on connection sensitivity. *arXiv preprint arXiv:1810.02340*, 2018.

540 Yun Li, Lin Niu, Xipeng Zhang, Kai Liu, Jianchen Zhu, and Zhanhui Kang. E-sparse: Boost-  
 541 ing the large language model inference through entropy-based n: M sparsity. *arXiv preprint*  
 542 *arXiv:2310.15929*, 2023.

543 Shiwei Liu, Lu Yin, Decebal Constantin Mocanu, and Mykola Pechenizkiy. Do we actually need  
 544 dense over-parameterization? in-time over-parameterization in sparse training. In *International*  
 545 *Conference on Machine Learning*, pp. 6989–7000. PMLR, 2021.

546 Vladimir Malinovskii, Denis Mazur, Ivan Ilin, Denis Kuznedelev, Konstantin Burlachenko, Kai Yi,  
 547 Dan Alistarh, and Peter Richtarik. Pv-tuning: Beyond straight-through estimation for extreme  
 548 llm compression. *arXiv preprint arXiv:2405.14852*, 2024.

549 Stephen Merity, Caiming Xiong, James Bradbury, and Richard Socher. Pointer sentinel mixture  
 550 models. *arXiv preprint arXiv:1609.07843*, 2016.

551 Todor Mihaylov, Peter Clark, Tushar Khot, and Ashish Sabharwal. Can a suit of armor conduct  
 552 electricity? a new dataset for open book question answering. *arXiv preprint arXiv:1809.02789*,  
 553 2018.

554 Decebal Constantin Mocanu, Elena Mocanu, Peter Stone, Phuong H Nguyen, Madeleine Gibescu,  
 555 and Antonio Liotta. Scalable training of artificial neural networks with adaptive sparse connec-  
 556 tivity inspired by network science. *Nature communications*, 9(1):2383, 2018.

557 Hesham Mostafa and Xin Wang. Parameter efficient training of deep convolutional neural networks  
 558 by dynamic sparse reparameterization. In *International Conference on Machine Learning*, pp.  
 559 4646–4655. PMLR, 2019.

560 Colin Raffel, Noam Shazeer, Adam Roberts, Katherine Lee, Sharan Narang, Michael Matena, Yanqi  
 561 Zhou, Wei Li, and Peter J Liu. Exploring the limits of transfer learning with a unified text-to-text  
 562 transformer. *Journal of machine learning research*, 21(140):1–67, 2020.

563 Keisuke Sakaguchi, Ronan Le Bras, Chandra Bhagavatula, and Yejin Choi. Winogrande: An adver-  
 564 sarial winograd schema challenge at scale. *Communications of the ACM*, 64(9):99–106, 2021.

565 Mingjie Sun, Zhuang Liu, Anna Bair, and J Zico Kolter. A simple and effective pruning approach  
 566 for large language models. In *The Twelfth International Conference on Learning Representations*,  
 567 2023.

568 Hugo Touvron, Thibaut Lavril, Gautier Izacard, Xavier Martinet, Marie-Anne Lachaux, Timothée  
 569 Lacroix, Baptiste Rozière, Naman Goyal, Eric Hambro, Faisal Azhar, et al. Llama: Open and  
 570 efficient foundation language models. *arXiv preprint arXiv:2302.13971*, 2023a.

571 Hugo Touvron, Louis Martin, Kevin Stone, Peter Albert, Amjad Almahairi, Yasmine Babaei, Niko-  
 572 lay Bashlykov, Soumya Batra, Prajjwal Bhargava, Shruti Bhosale, et al. Llama 2: Open founda-  
 573 tion and fine-tuned chat models. *arXiv preprint arXiv:2307.09288*, 2023b.

574 A Wang, A Singh, J Michael, F Hill, O Levy, and SR Bowman. Glue: A multi-task benchmark and  
 575 analysis platform for natural language understanding. *arxiv preprint arxiv: 180407461*, 2018.

576 Thomas Wolf, Lysandre Debut, Victor Sanh, Julien Chaumond, Clement Delangue, Anthony Moi,  
 577 Pierrick Cistac, Tim Rault, Rémi Louf, Morgan Funtowicz, et al. Transformers: State-of-the-art  
 578 natural language processing. *EMNLP 2020*, pp. 38, 2020.

579 Guangxuan Xiao, Ji Lin, Mickael Seznec, Hao Wu, Julien Demouth, and Song Han. Smoothquant:  
 580 Accurate and efficient post-training quantization for large language models. In *International*  
 581 *Conference on Machine Learning*, pp. 38087–38099. PMLR, 2023.

582 Rui Ye, Rui Ge, Xinyu Zhu, Jingyi Chai, Yixin Du, Yang Liu, Yanfeng Wang, and Siheng Chen.  
 583 Fedllm-bench: Realistic benchmarks for federated learning of large language models. *arXiv*  
 584 *preprint arXiv:2406.04845*, 2024.

585 Kai Yi, Nidham Gazagnadou, Peter Richtarik, and Lingjuan Lyu. Fedp3: Federated personalized  
 586 and privacy-friendly network pruning under model heterogeneity. *ICLR*, 2024.

594 Rowan Zellers, Ari Holtzman, Yonatan Bisk, Ali Farhadi, and Yejin Choi. Hellaswag: Can a ma-  
 595 chine really finish your sentence? *arXiv preprint arXiv:1905.07830*, 2019.

596

597 Aozhong Zhang, Naigang Wang, Yanxia Deng, Xin Li, Zi Yang, and Penghang Yin. Magr: Weight  
 598 magnitude reduction for enhancing post-training quantization. *Advances in neural information*  
 599 *processing systems*, 2024a.

600 Susan Zhang, Stephen Roller, Naman Goyal, Mikel Artetxe, Moya Chen, Shuohui Chen, Christo-  
 601 pher Dewan, Mona Diab, Xian Li, Xi Victoria Lin, et al. Opt: Open pre-trained transformer  
 602 language models. *arXiv preprint arXiv:2205.01068*, 2022a.

603

604 Yingtao Zhang, Haoli Bai, Haokun Lin, Jialin Zhao, Lu Hou, and Carlo Vittorio Cannistraci. Plug-  
 605 and-play: An efficient post-training pruning method for large language models. In *The Twelfth*  
 606 *International Conference on Learning Representations*, 2024b.

607 Yuxin Zhang, Mingbao Lin, Zhihang Lin, Yiting Luo, Ke Li, Fei Chao, Yongjian Wu, and Ron-  
 608 grong Ji. Learning best combination for efficient n: M sparsity. *Advances in Neural Information*  
 609 *Processing Systems*, 35:941–953, 2022b.

610 Yuxin Zhang, Lirui Zhao, Mingbao Lin, Yunyun Sun, Yiwu Yao, Xingjia Han, Jared Tanner, Shiwei  
 611 Liu, and Rongrong Ji. Dynamic sparse no training: Training-free fine-tuning for sparse llms.  
 612 *arXiv preprint arXiv:2310.08915*, 2023.

613

614 Aojun Zhou, Yukun Ma, Junnan Zhu, Jianbo Liu, Zhijie Zhang, Kun Yuan, Wenxiu Sun, and Hong-  
 615 sheng Li. Learning n: m fine-grained structured sparse neural networks from scratch. *arXiv*  
 616 *preprint arXiv:2102.04010*, 2021.

617 Xunyu Zhu, Jian Li, Yong Liu, Can Ma, and Weiping Wang. A survey on model compression  
 618 for large language models. *Transactions of the Association for Computational Linguistics*, 12:  
 619 1556–1577, 2024.

620

621

622

623

624

625

626

627

628

629

630

631

632

633

634

635

636

637

638

639

640

641

642

643

644

645

646

647

648	CONTENTS	
649		
650		
651	<b>1</b> <b>Introduction</b>	<b>1</b>
652		
653	<b>2</b> <b>Related Work</b>	<b>2</b>
654		
655	<b>3</b> <b>Symmetric Wanda</b>	<b>3</b>
656		
657	3.1 Prerequisites . . . . .	3
658	3.2 Symmetric Wanda: New Formulations . . . . .	4
659	3.3 From Relative Importance (RI) to RI Activation . . . . .	5
660	3.4 General Solution . . . . .	5
661	3.5 Enhanced Relative Importance Strategies . . . . .	5
662	3.5.1 Generalized $\ell_p$ -Norm . . . . .	6
663	3.5.2 Stochastic Relative Importance . . . . .	6
664	3.6 Training-Free Fine-Tuning . . . . .	6
665		
666		
667		
668		
669	<b>4</b> <b>Experiments</b>	<b>7</b>
670		
671	4.1 Efficiency of Stochastic Methods . . . . .	7
672	4.2 Training-Free Fine-Tuning Comparisons . . . . .	8
673		
674	<b>5</b> <b>Discussion, Limitations, and Future Work</b>	<b>9</b>
675		
676	<b>6</b> <b>Conclusion</b>	<b>9</b>
677		
678		
679	<b>A</b> <b>Missing Proofs</b>	<b>16</b>
680		
681	A.1 Proof of Lemma 3.1 . . . . .	16
682	A.2 Proof of Theorem 3.5 . . . . .	16
683	A.3 Proof of Lemma 3.7 . . . . .	17
684	A.4 Proof of Lemma 3.8 . . . . .	17
685	A.5 Proof of Lemma 3.9 . . . . .	18
686	A.6 Proof of Lemma 3.10 . . . . .	18
687		
688		
689		
690	<b>B</b> <b>Symmetric Wanda Variant with Squared Frobenius Norms</b>	<b>20</b>
691		
692	<b>C</b> <b>Insights on Sensitivity, Activation, and Sparsity</b>	<b>21</b>
693		
694	C.1 Column and Row Sensitivity . . . . .	21
695	C.2 Benefits of Square Root Input Activation . . . . .	22
696	C.3 Various Unstructured Sparsity Ratios . . . . .	22
697		
698		
699	<b>D</b> <b>Additional Experiments</b>	<b>23</b>
700		
701	D.1 Implementation Details . . . . .	23
	D.2 Optimal $\ell_p$ Norm . . . . .	23

702	D.3 $\ell_p$ Norm Re-weighting . . . . .	24
703		
704	D.4 Influence of Sampling Ratios . . . . .	24
705	D.5 Analysis of $R^2$ -DSnoT Hyperparameters . . . . .	25
706		
707		
708		
709		
710		
711		
712		
713		
714		
715		
716		
717		
718		
719		
720		
721		
722		
723		
724		
725		
726		
727		
728		
729		
730		
731		
732		
733		
734		
735		
736		
737		
738		
739		
740		
741		
742		
743		
744		
745		
746		
747		
748		
749		
750		
751		
752		
753		
754		
755		

756  
757

## BROADER IMPACT

758  
759  
760  
761  
762  
763

This work proposes a unified symmetric formulation and a set of practical algorithms for post-training pruning and compression of LLMs. By improving the efficiency of existing models without retraining, our methods lower the computational barrier for running LLMs, enabling broader accessibility in academic, industrial, and resource-constrained settings. This could benefit smaller research labs, educational institutions, and applications where deploying full-scale models is infeasible due to cost or hardware limitations.

764  
765  
766  
767

On the positive side, this work contributes to democratizing access to powerful language models, potentially accelerating innovation in under-resourced regions and facilitating energy-efficient deployment on edge devices. In addition, our training-free fine-tuning approach promotes sustainability by reducing the need for compute-heavy finetuning procedures.

768  
769  
770  
771  
772  
773  
774

However, as with any work that enhances the deployability of LLMs, this research could also lower the barrier for misuse. Compressed models may be used in applications that propagate misinformation, generate spam, or amplify social biases embedded in the base models. Since our methods operate on publicly available LLMs, they inherit the original model's limitations and risks. We do not explicitly address fairness, robustness, or misuse detection in this work, and we encourage future research to consider safeguards, such as watermarking, usage monitoring, or alignment-aware pruning, to mitigate potential harms.

775  
776  
777

Overall, this work aims to improve the accessibility and computational efficiency of language models, while recognizing the importance of responsible deployment in real-world applications.

778  
779  
780  
781  
782  
783  
784  
785  
786  
787  
788  
789  
790  
791  
792  
793  
794  
795  
796  
797  
798  
799  
800  
801  
802  
803  
804  
805  
806  
807  
808  
809

## A MISSING PROOFS

## A.1 PROOF OF LEMMA 3.1

By using the definition of  $g(\widetilde{\mathbf{W}})$  in Equation (InpRecon), we have

$$\begin{aligned}
 g(\widetilde{\mathbf{W}}) &= \sqrt{\sum_{k=1}^c \left\| \mathbf{X} (\widetilde{\mathbf{W}}_{:k} - \mathbf{W}_{:k}) \right\|_2^2} + \sqrt{\sum_{j=1}^b \left\| (\widetilde{\mathbf{W}}_{j:} - \mathbf{W}_{j:}) \mathbf{Y} \right\|_2^2} \\
 &= \sqrt{\sum_{k=1}^c \sum_{i=1}^a \left( \mathbf{X}_{i:} (\widetilde{\mathbf{W}}_{:k} - \mathbf{W}_{:k}) \right)^2} + \sqrt{\sum_{j=1}^b \sum_{l=1}^d \left( (\widetilde{\mathbf{W}}_{j:} - \mathbf{W}_{j:}) \mathbf{Y}_{:l} \right)^2} \\
 &= \sqrt{\sum_{k=1}^c \sum_{i=1}^a \left( \sum_{j=1}^b \mathbf{X}_{ij} (\widetilde{\mathbf{W}}_{jk} - \mathbf{W}_{jk}) \right)^2} + \sqrt{\sum_{j=1}^b \sum_{l=1}^d \left( \sum_{k=1}^c (\widetilde{\mathbf{W}}_{jk} - \mathbf{W}_{jk}) \mathbf{Y}_{kl} \right)^2}
 \end{aligned}$$

Now say we want to prune away just a single weight  $\mathbf{W}_{jk}$ . That is, we want to set  $\widetilde{\mathbf{W}}_{jk} = 0$  and  $\widetilde{\mathbf{W}}_{j'k'} = \mathbf{W}_{j'k'}$  for all  $(j', k') \neq (j, k)$ . For such a weight matrix  $\widetilde{\mathbf{W}}_{jk}$  the expression for  $f(\widetilde{\mathbf{W}})$  simplifies to

$$\begin{aligned}
 g(\widetilde{\mathbf{W}}) &= \sum_{i=1}^a \left( \sum_{j'=1}^b \mathbf{X}_{ij'} (\widetilde{\mathbf{W}}_{j'k} - \mathbf{W}_{j'k}) \right)^2 + \sum_{l=1}^d \left( \sum_{k'=1}^c (\widetilde{\mathbf{W}}_{jk'} - \mathbf{W}_{jk'}) \mathbf{Y}_{k'l} \right)^2 \\
 &= \sqrt{\sum_{i=1}^a \left( \mathbf{X}_{ij} (\widetilde{\mathbf{W}}_{jk} - \mathbf{W}_{jk}) + \sum_{j' \neq j} \mathbf{X}_{ij'} (\widetilde{\mathbf{W}}_{j'k} - \mathbf{W}_{j'k}) \right)^2} \\
 &\quad + \sqrt{\sum_{l=1}^d \left( (\widetilde{\mathbf{W}}_{jk} - \mathbf{W}_{jk}) \mathbf{Y}_{kl} + \sum_{k' \neq k} (\widetilde{\mathbf{W}}_{jk} - \mathbf{W}_{jk}) \mathbf{Y}_{k'l} \right)^2} \\
 &= \sqrt{\sum_{i=1}^a \left( \mathbf{X}_{ij} (0 - \mathbf{W}_{jk}) + \sum_{j' \neq j} \mathbf{X}_{ij'} \underbrace{(\mathbf{W}_{j'k} - \mathbf{W}_{j'k})}_{=0} \right)^2} \\
 &\quad + \sqrt{\sum_{l=1}^d \left( (0 - \mathbf{W}_{jk}) \mathbf{Y}_{kl} + \sum_{k' \neq k} \underbrace{(\widetilde{\mathbf{W}}_{jk} - \mathbf{W}_{jk}) \mathbf{Y}_{kl}}_{=0} \right)^2} \\
 &= \sqrt{\sum_{i=1}^a (-\mathbf{X}_{ij} \mathbf{W}_{jk})^2} + \sqrt{\sum_{l=1}^d (-\mathbf{W}_{jk} \mathbf{Y}_{kl})^2} \\
 &= \sqrt{\sum_{i=1}^a \mathbf{X}_{ij}^2 \mathbf{W}_{jk}^2} + \sqrt{\sum_{l=1}^d \mathbf{W}_{jk}^2 \mathbf{Y}_{kl}^2} \\
 &= |\mathbf{W}_{jk}| (\|\mathbf{X}_{:j}\|_2 + \|\mathbf{Y}_{k:}\|_2) := \mathbf{S}_{jk}.
 \end{aligned}$$

## A.2 PROOF OF THEOREM 3.5

- Assume it is possible to choose matrices  $\mathbf{X} \in \mathbb{R}^{a \times b}$  and  $\mathbf{Y} \in \mathbb{R}^{c \times d}$  such that the identity

$$\|\mathbf{X}_{:k}\|_2 + \|\mathbf{Y}_{j:}\|_2 = \alpha_{jk} := \frac{1}{\|\mathbf{W}_{j:}\|_1} + \frac{1}{\|\mathbf{W}_{:k}\|_1} \quad (7)$$

864 holds for all  $j, k$ . This is always possible!  
 865 Indeed, if we choose  $a = b$ , and let the  $j$ -th row of  $\mathbf{X}$  be of the form  $\mathbf{X}_{:j} := t_j(1; \dots; 1) \in$   
 866  $\mathbb{R}^{b \times 1}$ , where  $t_j = \frac{1}{\sqrt{b}\|\mathbf{W}_{j:}\|_1}$ , then  $\|\mathbf{X}_{:j}\|_2 = t_j\sqrt{b} = \frac{1}{\|\mathbf{W}_{j:}\|_1}$ .  
 867 Similarly, if we choose  $d = c$ , and let the  $k$ -th column of  $\mathbf{Y}$  be of the form  $\mathbf{Y}_{:k} :=$   
 868  $s_k(1, \dots, 1) \in \mathbb{R}^{1 \times c}$ , where  $s_k = \frac{1}{\sqrt{c}\|\mathbf{W}_{:k}\|_1}$ , then  $\|\mathbf{Y}_{:k}\|_2 = s_k\sqrt{c} = \frac{1}{\|\mathbf{W}_{:k}\|_1}$ .  
 869 So, Equation (7) holds. In this case, our score matrix Equation (1) reduces to the plug-and-  
 870 play method RIA (Zhang et al., 2024b).  
 871

- 873 • Another (even simpler) possibility for constructing matrices  $\mathbf{X}, \mathbf{Y}$  such that Equation (7)  
 874 holds is as follows. Let  $a = b$ , and let  $\mathbf{X} = \text{Diag}(\|\mathbf{W}_{1:}\|_1^{-1}, \dots, \|\mathbf{W}_{b:}\|_1^{-1})$ . Clearly, for  
 875 all  $j = 1, \dots, b$  we have  $\|\mathbf{X}_{:j}\|_2 = \frac{1}{\|\mathbf{W}_{j:}\|_1}$ .  
 876 Similarly, let  $d = c$ , and let  $\mathbf{Y} = \text{Diag}(\|\mathbf{W}_{:1}\|_1^{-1}, \dots, \|\mathbf{W}_{:c}\|_1^{-1})$ . Clearly, for all  $k =$   
 877  $1, \dots, c$ , we have  $\|\mathbf{Y}_{:k}\|_2 = \frac{1}{\|\mathbf{W}_{:k}\|_1}$ .  
 878 Therefore,  $\|\mathbf{X}_{:j}\|_2 + \|\mathbf{Y}_{:k}\|_2 = \frac{1}{\|\mathbf{W}_{j:}\|_1} + \frac{1}{\|\mathbf{W}_{:k}\|_1}$  for all  $j, k$ . So again, our score matrix  
 879 (1) reduces to the plug-and-play method in Zhang et al. (2024b).  
 880

### 882 A.3 PROOF OF LEMMA 3.7

884 Recall that in Section 3.4  $\mathbf{D}_{\mathbf{X}} \in \mathbb{R}^{b \times b}$  and  $\mathbf{D}_{\mathbf{Y}} \in \mathbb{R}^{c \times c}$  are diagonal matrices with entries defined  
 885 as  $(\mathbf{D}_{\mathbf{X}})_{ii} = x_i = \|\mathbf{W}_{i:}\|_1^{-1}$  and  $(\mathbf{D}_{\mathbf{Y}})_{ii} = y_i = \|\mathbf{W}_{:i}\|_1^{-1}$  respectively, and  $\mathbf{A} \in \mathbb{R}^{a \times b}$  and  
 886  $\mathbf{B} \in \mathbb{R}^{c \times d}$  are arbitrary matrices. We first compute  $\mathbf{AD}_{\mathbf{X}}$ . This product scales each column of  $\mathbf{A}$   
 887 by the corresponding  $x_i$ . Specifically, for the  $j$ -th column, this operation is expressed as:

$$888 \quad (\mathbf{AD}_{\mathbf{X}})_{:j} = x_j \mathbf{A}_{:j}. \\ 889$$

890 The  $\ell_2$ -norm of this column is then given by:

$$891 \quad \|(\mathbf{AD}_{\mathbf{X}})_{:j}\|_2 = x_j \|\mathbf{A}_{:j}\|_2 = \frac{\|\mathbf{A}_{:j}\|_2}{\|\mathbf{W}_{j:}\|_1}. \\ 892 \\ 893$$

894 Next, we compute  $\mathbf{D}_{\mathbf{Y}}\mathbf{B}$ . In this computation, each row of  $\mathbf{B}$  is scaled by the corresponding  $y_i$ . For  
 895 the  $k$ -th row, the scaling is represented as:

$$896 \quad (\mathbf{D}_{\mathbf{Y}}\mathbf{B})_{k:} = y_k \mathbf{B}_{k:}. \\ 897$$

898 The  $\ell_2$ -norm of this row is:

$$899 \quad \|(\mathbf{D}_{\mathbf{Y}}\mathbf{B})_{k:}\|_2 = y_k \|\mathbf{B}_{k:}\|_2 = \frac{\|\mathbf{B}_{k:}\|_2}{\|\mathbf{W}_{:k}\|_1}. \\ 900 \\ 901$$

902 Finally, we consider the sum of these norms:

$$903 \quad \|(\mathbf{AD}_{\mathbf{X}})_{:j}\|_2 + \|(\mathbf{D}_{\mathbf{Y}}\mathbf{B})_{k:}\|_2 = \frac{\|\mathbf{A}_{:j}\|_2}{\|\mathbf{W}_{j:}\|_1} + \frac{\|\mathbf{B}_{k:}\|_2}{\|\mathbf{W}_{:k}\|_1}. \\ 904 \\ 905 \\ 906$$

907 The first term involves scaling the  $j$ -th column of  $\mathbf{A}$  by  $x_j$ , with the resulting norm being the original  
 908 column norm divided by the  $\ell_1$ -norm of the corresponding weights in  $\mathbf{W}$ . Similarly, the second term  
 909 scales the  $k$ -th row of  $\mathbf{B}$  by  $y_k$ , with the resulting norm also being the original row norm divided by  
 910 the  $\ell_1$ -norm of the corresponding weights in  $\mathbf{W}$ .

### 911 A.4 PROOF OF LEMMA 3.8

912 We aim to construct  $\mathbf{X}_{:j}$  to be proportional to  $\mathbf{W}_{j:}^\top$ . A natural choice is to set

$$913 \quad \mathbf{X}_{:j} = c \cdot \mathbf{W}_{j:}^\top, \\ 914$$

915 where  $c$  is a scalar to be determined. A similar condition applies when considering  $\mathbf{Y}_{k:}$ . The central  
 916 task is to compute the corresponding scaling factor  $c$  for both  $\mathbf{X}$  and  $\mathbf{Y}$ .

918 To determine  $c$ , we choose it such that  
 919  
 920

$$\|\mathbf{X}_{:j}\|_2 = \|c \cdot \mathbf{W}_{j:}^\top\|_2 = \|\mathbf{W}_{j:}\|_p^{-1}.$$

921 We now compute the  $\ell_2$ -norm of  $\mathbf{X}_{:j}$ :  
 922  
 923

$$\|c \cdot \mathbf{W}_{j:}^\top\|_2 = |c| \cdot \|\mathbf{W}_{j:}^\top\|_2 = |c| \cdot \|\mathbf{W}_{j:}\|_2.$$

925 Setting this equal to  $\|\mathbf{W}_{j:}\|_p^{-1}$ , we have:  
 926  
 927

$$|c| \cdot \|\mathbf{W}_{j:}\|_2 = \|\mathbf{W}_{j:}\|_p^{-1}.$$

928 Solving for  $c$ , we obtain:  
 929  
 930

$$c = \frac{1}{\|\mathbf{W}_{j:}\|_p} \cdot \frac{1}{\|\mathbf{W}_{j:}\|_2}.$$

931 Using this value of  $c$ , we define  $\mathbf{X}_{:j}$  as:  
 932  
 933

$$\mathbf{X}_{:j} = \frac{1}{\|\mathbf{W}_{j:}\|_p} \cdot \frac{1}{\|\mathbf{W}_{j:}\|_2} \cdot \mathbf{W}_{j:}^\top.$$

934 This construction ensures that  
 935  
 936

$$\|\mathbf{X}_{:j}\|_2 = \|\mathbf{W}_{j:}\|_p^{-1}.$$

937 Similarly, for  $\mathbf{Y}$ , we have:  
 938  
 939

$$\mathbf{Y}_{k:} = \frac{1}{\|\mathbf{W}_{:k}\|_p} \cdot \frac{1}{\|\mathbf{W}_{:k}\|_2} \cdot \mathbf{W}_{:k}^\top,$$

940 which satisfies Equation (3).  
 941  
 942

943 By combining these results, we conclude the proof of Lemma 3.8.  
 944  
 945

#### A.5 PROOF OF LEMMA 3.9

946 Let  $\mathbf{u}$  be any unit vector in  $\ell_2$ -norm, i.e.,  $\|\mathbf{u}\|_2 = 1$ . Construct  $\mathbf{X}_{:j} = \|\mathbf{W}_{j:}\|_p^{-1} \mathbf{u}$ . Then by using  
 947 the definition of the  $\ell_2$ -norm, we have  
 948

$$\|\mathbf{X}_{:j}\|_2 = \|\|\mathbf{W}_{j:}\|_p^{-1} \mathbf{u}\|_2 = \left\| \|\mathbf{W}_{j:}\|_p^{-1} \right\| \|\mathbf{u}\|_2 = \|\mathbf{W}_{j:}\|_p^{-1} \cdot 1 = \|\mathbf{W}_{j:}\|_p^{-1}.$$

949 Hence, we obtain  $\|\mathbf{X}_{:j}\|_2 = \|\mathbf{W}_{j:}\|_p^{-1}$ , which is exactly as desired.  
 950  
 951

952 Similarly, let  $\mathbf{v}$  be any unit vector in  $\ell_2$ -norm, we have  $|\mathbf{W}_{jk}| \cdot \|\mathbf{W}_{:k}\|_p^{-1}$ .  
 953  
 954

955 Put them together, we prove Lemma 3.9.  
 956  
 957

#### A.6 PROOF OF LEMMA 3.10

958 Given that  $\mathbf{X}_{:j}$  and  $\mathbf{Y}_{k:}$  are vectors to be constructed,  $\mathbf{W}$  is a matrix, and  $S_j$  and  $S_k$  are randomly  
 959 sampled index sets from the  $j$ -th row and  $k$ -th column of  $\mathbf{W}$ , respectively, each with cardinality  $\tau$ ,  
 960 our task is to construct  $\mathbf{X}_{:j}$  and  $\mathbf{Y}_{k:}$  with specific norms. Specifically, the goal is to construct  $\mathbf{X}_{:j}$   
 961 and  $\mathbf{Y}_{k:}$  such that:  
 962

$$\|\mathbf{X}_{:j}\|_2 + \|\mathbf{Y}_{k:}\|_2 = \frac{1}{\|\mathbf{W}_{j:S_j}\|_1} + \frac{1}{\|\mathbf{W}_{S_k:k}\|_1},$$

963 where  $\mathbf{W}_{j:S_j}$  denotes the entries of the  $j$ -th row of  $\mathbf{W}$  at indices in  $S_j$ , and  $\mathbf{W}_{S_k:k}$  denotes the  
 964 entries of the  $k$ -th column of  $\mathbf{W}$  at indices in  $S_k$ .  
 965  
 966

967 We first define the support vector  $\mathbf{e}_{S_j}$  of appropriate size (equal to the number of rows in  $\mathbf{X}$ ) as:  
 968  
 969

$$(\mathbf{e}_{S_j})_i = \begin{cases} \frac{1}{\sqrt{\tau}}, & \text{if } i \in S_j, \\ 0, & \text{otherwise.} \end{cases}$$

972 The vector  $\mathbf{e}_{S_j}$  has non-zero entries only at indices in  $S_j$ , each equal to  $\frac{1}{\sqrt{\tau}}$ , ensuring that the  $\ell_2$ -  
 973 norm of  $\mathbf{e}_{S_j}$  is 1:  
 974

$$975 \quad 976 \quad 977 \quad \|\mathbf{e}_{S_j}\|_2 = \sqrt{\sum_{i \in S_j} \left(\frac{1}{\sqrt{\tau}}\right)^2} = \sqrt{\tau \cdot \left(\frac{1}{\sqrt{\tau}}\right)^2} = 1.$$

978 To construct  $\mathbf{X}_{:j}$ , we set:  
 979

$$980 \quad \mathbf{X}_{:j} = \frac{1}{\|\mathbf{W}_{j:S_j}\|_1} \cdot \mathbf{e}_{S_j}.$$

982 A basic verification shows that the  $\ell_2$ -norm of  $\mathbf{X}_{:j}$  is:  
 983

$$984 \quad 985 \quad 986 \quad \|\mathbf{X}_{:j}\|_2 = \frac{1}{\|\mathbf{W}_{j:S_j}\|_1} \cdot \|\mathbf{e}_{S_j}\|_2 = \frac{1}{\|\mathbf{W}_{j:S_j}\|_1} \cdot 1 = \frac{1}{\|\mathbf{W}_{j:S_j}\|_1}.$$

987 Similarly, we define the support vector  $\mathbf{e}_{S_k}$  of appropriate size (equal to the number of columns in  
 988  $\mathbf{Y}$ ) as:  
 989

$$990 \quad 991 \quad (\mathbf{e}_{S_k})_i = \begin{cases} \frac{1}{\sqrt{\tau}}, & \text{if } i \in S_k, \\ 0, & \text{otherwise.} \end{cases}$$

992 To construct  $\mathbf{Y}_{k:}$ , we set:  
 993

$$994 \quad \mathbf{Y}_{k:} = \frac{1}{\|\mathbf{W}_{S_k:k}\|_1} \cdot \mathbf{e}_{S_k}^\top.$$

996 Adding the norms:  
 997

$$998 \quad 999 \quad \|\mathbf{X}_{:j}\|_2 + \|\mathbf{Y}_{k:}\|_2 = \frac{1}{\|\mathbf{W}_{j:S_j}\|_1} + \frac{1}{\|\mathbf{W}_{S_k:k}\|_1},$$

1000 which matches the desired expression.  
 1001

### 1002 Alternative construction using $\ell_1$ and $\ell_2$ norms.

1003 By definition:

$$1004 \quad 1005 \quad 1006 \quad \|\mathbf{W}_{j:S_j}\|_1 = \sum_{i \in S_j} |w_{ji}|, \quad \|\mathbf{W}_{j:S_j}\|_2 = \sqrt{\sum_{i \in S_j} w_{ji}^2}.$$

1007 We can construct  $\mathbf{X}_{:j}$  as:  
 1008

$$1009 \quad 1010 \quad \mathbf{X}_{:j} = \frac{1}{\|\mathbf{W}_{j:S_j}\|_1} \cdot \frac{1}{\|\mathbf{W}_{j:S_j}\|_2} \cdot \mathbf{W}_{j:S_j}^\top,$$

1011 where  $\mathbf{W}_{j:S_j}^\top$  is a vector with entries:  
 1012

$$1013 \quad 1014 \quad 1015 \quad (\mathbf{W}_{j:S_j}^\top)_i = \begin{cases} w_{ji}, & \text{if } i \in S_j, \\ 0, & \text{otherwise.} \end{cases}$$

1016 Similarly, we can construct  $\mathbf{Y}_{k:}$  as:  
 1017

$$1018 \quad 1019 \quad \mathbf{Y}_{k:} = \frac{1}{\|\mathbf{W}_{S_k:k}\|_1} \cdot \frac{1}{\|\mathbf{W}_{S_k:k}\|_2} \cdot \mathbf{W}_{S_k:k}^\top,$$

1020 where  $\mathbf{W}_{S_k:k}^\top$  is a vector with entries:  
 1021

$$1022 \quad 1023 \quad 1024 \quad (\mathbf{W}_{S_k:k}^\top)_i = \begin{cases} w_{ik}, & \text{if } i \in S_k, \\ 0, & \text{otherwise.} \end{cases}$$

1025 Putting everything together, we prove Lemma 3.10.

1026 B SYMMETRIC WANDA VARIANT WITH SQUARED FROBENIUS NORMS  
10271028 Choose  $\varepsilon \in (0, 1]$ . Given  $\mathbf{X} \in \mathbb{R}^{a \times b}$ ,  $\mathbf{W} \in \mathbb{R}^{b \times c}$  and  $\mathbf{Y} \in \mathbb{R}^{c \times d}$ , define  
1029

1030 1031 
$$g'(\widetilde{\mathbf{W}}) := \|\mathbf{X}(\widetilde{\mathbf{W}} - \mathbf{W})\|_F^2 + \|(\widetilde{\mathbf{W}} - \mathbf{W})\mathbf{Y}\|_F^2,$$
  
1032

1033 and consider solving the problem  
1034

1035 
$$\text{minimize } g'(\widetilde{\mathbf{W}}) \quad s.t. \quad \text{Mem}(\widetilde{\mathbf{W}}) \leq \varepsilon \text{Mem}(\mathbf{W}), \widetilde{\mathbf{W}} \in \mathbb{R}^{b \times c}.$$
  
1036

1037 Note that  
1038

1039  
1040 
$$g'(\widetilde{\mathbf{W}}) = \sum_{k=1}^c \left\| \mathbf{X} \left( \widetilde{\mathbf{W}}_{:k} - \mathbf{W}_{:k} \right) \right\|_2^2 + \sum_{j=1}^b \left\| \left( \widetilde{\mathbf{W}}_{j:} - \mathbf{W}_{j:} \right) \mathbf{Y} \right\|_2^2$$
  
1041  
1042  
1043 
$$= \sum_{k=1}^c \sum_{i=1}^a \left( \mathbf{X}_{i:} \left( \widetilde{\mathbf{W}}_{:k} - \mathbf{W}_{:k} \right) \right)^2 + \sum_{j=1}^b \sum_{l=1}^d \left( \left( \widetilde{\mathbf{W}}_{j:} - \mathbf{W}_{j:} \right) \mathbf{Y}_{:l} \right)^2$$
  
1044  
1045  
1046 
$$= \sum_{k=1}^c \sum_{i=1}^a \left( \sum_{j=1}^b \mathbf{X}_{ij} \left( \widetilde{\mathbf{W}}_{jk} - \mathbf{W}_{jk} \right) \right)^2 + \sum_{j=1}^b \sum_{l=1}^d \left( \sum_{k=1}^c \left( \widetilde{\mathbf{W}}_{jk} - \mathbf{W}_{jk} \right) \mathbf{Y}_{kl} \right)^2$$
  
1047  
1048  
1049

1050 Now say we want to prune away just a single weight  $\mathbf{W}_{jk}$ . That is, we want to set  $\widetilde{\mathbf{W}}_{jk} = 0$  and  
1051  $\widetilde{\mathbf{W}}_{j'k'} = \mathbf{W}_{j'k'}$  for all  $(j', k') \neq (j, k)$ . For such a weight matrix  $\widetilde{\mathbf{W}}_{jk}$  the expression for  $g'(\widetilde{\mathbf{W}})$   
1052 simplifies to  
1053

1054  
1055 
$$g'(\widetilde{\mathbf{W}}) = \sum_{i=1}^a \left( \sum_{j'=1}^b \mathbf{X}_{ij'} \left( \widetilde{\mathbf{W}}_{j'k} - \mathbf{W}_{j'k} \right) \right)^2 + \sum_{l=1}^d \left( \sum_{k'=1}^c \left( \widetilde{\mathbf{W}}_{jk'} - \mathbf{W}_{jk'} \right) \mathbf{Y}_{k'l} \right)^2$$
  
1056  
1057  
1058  
1059 
$$= \sum_{i=1}^a \left( \mathbf{X}_{ij} \left( \widetilde{\mathbf{W}}_{jk} - \mathbf{W}_{jk} \right) + \sum_{j' \neq j} \mathbf{X}_{ij'} \left( \widetilde{\mathbf{W}}_{j'k} - \mathbf{W}_{j'k} \right) \right)^2$$
  
1060  
1061  
1062 
$$+ \sum_{l=1}^d \left( \left( \widetilde{\mathbf{W}}_{jk} - \mathbf{W}_{jk} \right) \mathbf{Y}_{kl} + \sum_{k' \neq k} \left( \widetilde{\mathbf{W}}_{jk} - \mathbf{W}_{jk} \right) \mathbf{Y}_{kl} \right)^2$$
  
1063  
1064  
1065  
1066 
$$= \sum_{i=1}^a (\mathbf{X}_{ij} (0 - \mathbf{W}_{jk}) + \sum_{j' \neq j} \mathbf{X}_{ij'} \underbrace{(\mathbf{W}_{j'k} - \mathbf{W}_{j'k})}_{=0})^2 + \sum_{l=1}^d ((0 - \mathbf{W}_{jk}) \mathbf{Y}_{kl} + \sum_{k' \neq k} \underbrace{(\widetilde{\mathbf{W}}_{jk} - \mathbf{W}_{jk}) \mathbf{Y}_{kl}}_{=0})^2$$
  
1067  
1068  
1069  
1070 
$$= \sum_{i=1}^a (-\mathbf{X}_{ij} \mathbf{W}_{jk})^2 + \sum_{l=1}^d (-\mathbf{W}_{jk} \mathbf{Y}_{kl})^2$$
  
1071  
1072  
1073 
$$= \sum_{i=1}^a \mathbf{X}_{ij}^2 \mathbf{W}_{jk}^2 + \sum_{l=1}^d \mathbf{W}_{jk}^2 \mathbf{Y}_{kl}^2$$
  
1074  
1075  
1076 
$$= \mathbf{W}_{jk}^2 \left( \|\mathbf{X}_{:j}\|_2^2 + \|\mathbf{Y}_{k:}\|_2^2 \right) := \mathbf{S}_{jk}^2.$$
  
1077

1078 Our proposal is to choose entry  $(j, k)$  which the smallest score  $\mathbf{S}_{jk}$ . Special cases:  
10791. If we choose  $\mathbf{X} = \mathbf{0} \in \mathbb{R}^{a \times b}$ , then our pruning method reduces to "output" Wanda:

1080  
1081  
1082

$$\mathbf{S}_{jk} := |\mathbf{W}_{jk}| \|\mathbf{Y}_{k:}\|_2$$

1083 2. If we choose  $\mathbf{Y} = \mathbf{0} \in \mathbb{R}^{c \times d}$ , then our pruning method reduces to "input" Wanda:

1084

1085

1086

$$\mathbf{S}_{jk} := |\mathbf{W}_{jk}| \|\mathbf{X}_{:j}\|_2.$$

1087

1088

1089

3. If we choose  $\mathbf{X} = \mathbf{W}^\top \in \mathbb{R}^{c \times b}$  ( $a = c$ ) and  $\mathbf{Y} = \mathbf{W}^\top \in \mathbb{R}^{c \times b}$  ( $d = b$ ), then our score matrix becomes

1090

1091

1092

$$\mathbf{S}_{jk} \stackrel{(27)}{=} |\mathbf{W}_{jk}| \sqrt{\|\mathbf{X}_{:j}\|_2^2 + \|\mathbf{Y}_{k:}\|_2^2} = |\mathbf{W}_{jk}| \sqrt{\|\mathbf{W}_{j:}\|_2^2 + \|\mathbf{W}_{:k}\|_2^2}$$

1093

1094

Letting  $\mathbf{G}_{jk}^2 := \frac{1}{b+c} \left( \|\mathbf{W}_{j:}\|_2^2 + \|\mathbf{W}_{:k}\|_2^2 \right)$ , note that

1095

1096

1097

1098

1099

1100

1101

1102

1103

1104

1105

1106

1107

1108

1109

1110

1111

$$\begin{aligned} \|\mathbf{G}\|_F^2 &= \sum_{j=1}^b \sum_{k=1}^c \mathbf{G}_{jk}^2 \\ &= \frac{1}{b+c} \sum_{j=1}^b \sum_{k=1}^c \left( \|\mathbf{W}_{j:}\|_2^2 + \|\mathbf{W}_{:k}\|_2^2 \right) \\ &= \frac{1}{b+c} \left( \sum_{j=1}^b \sum_{k=1}^c \|\mathbf{W}_{j:}\|_2^2 + \sum_{k=1}^c \sum_{j=1}^b \|\mathbf{W}_{:k}\|_2^2 \right) \\ &= \frac{1}{b+c} \left( c \sum_{j=1}^b \|\mathbf{W}_{j:}\|_2^2 + b \sum_{k=1}^c \|\mathbf{W}_{:k}\|_2^2 \right) \\ &= \frac{1}{b+c} (c \|\mathbf{W}\|_F^2 + b \|\mathbf{W}\|_F^2) \\ &= \|\mathbf{W}\|_F^2 \end{aligned}$$

1112

Clearly,

1113

1114

1115

1116

1117

$$\frac{\mathbf{S}_{jk}^2}{(b+c)\|\mathbf{W}\|_F^2} = \frac{\mathbf{W}_{jk}^2 \mathbf{G}_{jk}^2}{\|\mathbf{W}\|_F^2}$$

1118

4. Assume it is possible to choose matrices  $\mathbf{X} \in \mathbb{R}^{a \times b}$  and  $\mathbf{Y} \in \mathbb{R}^{c \times d}$  such that the identity

1119

1120

1121

1122

$$\sqrt{\|\mathbf{X}_{:j}\|_2^2 + \|\mathbf{Y}_{:k}\|_2^2} = \alpha_{jk} := \frac{1}{\|\mathbf{W}_{j:}\|_1} + \frac{1}{\|\mathbf{W}_{:k}\|_1}$$

1123

1124

holds for all  $j, k$  (note that this is not always possible!). In this case, our score matrix reduces to the plug-and-play method of [Zhang et al. \(2024b\)](#).

1125

1126

## C INSIGHTS ON SENSITIVITY, ACTIVATION, AND SPARSITY

1127

1128

## C.1 COLUMN AND ROW SENSITIVITY

1129

1130

1131

1132

1133

Compared with the Wanda design, RIA accounts for the relative importance of both rows and columns. However, it remains unclear whether columns and rows contribute equally to RIA's performance improvements. To investigate this, we conducted an extensive analysis of the significance of column-wise and row-wise relative importance, with the results shown in Table 5. A key finding is that the sum of the columns has more impact on performance, indicating greater importance.

1134 Table 5: Perplexity scores on Wikitext-2, accounting for various norm  $\alpha$  values and column & row  
 1135 sensitivity, with a sparsity ratio 50%.

1136

Model	LlaMA2-7b				LlaMA2-13b				LlaMA3-8b				OPT-1.3b				
	$\alpha$	0	0.5	1	2	0	0.5	1	2	0	0.5	1	2	0	0.5	1	2
Dense		5.47				4.88				6.14				14.62			
Wanda	16.03	7.60	7.79	8.66	6.83	6.17	6.28	7.15	205.44	10.66	10.81	12.98	1712.39	22.14	22.19	24.74	
Col-Sum	11.59	<b>6.83</b>	6.91	7.46	6.39	<b>5.87</b>	5.96	6.55	59.41	9.53	9.69	12.01	1062.66	<b>18.28</b>	18.41	22.25	
Row-Sum	14.93	7.49	7.51	8.01	6.74	6.13	6.24	7.01	17.80	10.50	10.55	11.79	141.92	22.09	22.47	26.62	
RIA	7.39	<b>6.81</b>	6.88	7.37	5.95	<b>5.93</b>	5.95	6.56	12.07	<b>9.34</b>	<b>9.44</b>	10.67	64.70	<b>18.08</b>	18.94	23.39	

1142

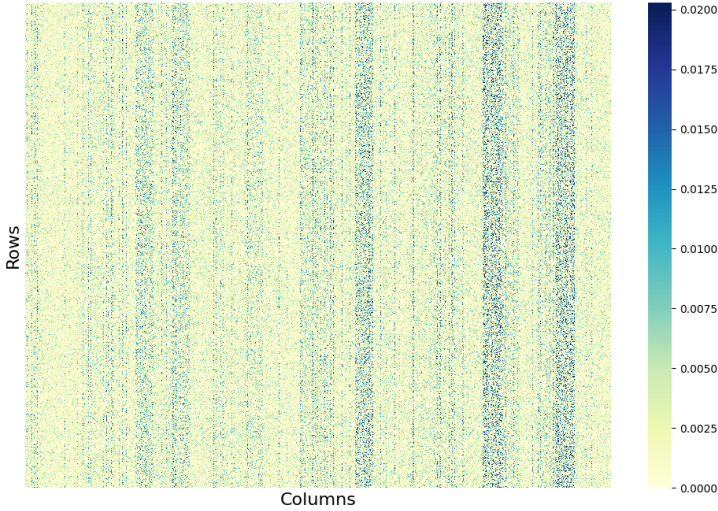


Figure 1: Visualization of the dense weight matrix in LLaMA2-7b.

1163

To provide further insights, we visualized the heatmap of a randomly selected dense weight matrix from LLaMA2-7b, as illustrated in Figure 1. The heatmap displays stripe-like patterns, indicating column-specific structures where certain columns show significantly higher activations, forming distinct stripes. This observation suggests that normalizing by rows effectively balances these disparities. In cases where the rows within a specific column already exhibit relatively uniform distributions, normalization over rows may not be necessary. Thus, column normalization alone might suffice to balance the contributions of output neurons, especially when some columns dominate due to large absolute values.

1171

## C.2 BENEFITS OF SQUARE ROOT INPUT ACTIVATION

1173

In the design of Wanda (Sun et al., 2023), the power factor  $\alpha$  applied to input activations is set to 1, whereas in RIA (Zhang et al., 2024b),  $\alpha$  is adjusted to 0.5. In this study, we systematically explore the impact of varying the power factor on input activations, with detailed results presented in Table 5. An  $\alpha$  value of 0 implies that no activation is considered in generating the pruning matrix. Our findings consistently show that incorporating input activation improves performance in terms of perplexity. Notably,  $\alpha = 0.5$  proved optimal across various methods, underscoring the advantages of reducing the magnitude of input activations. We attribute this improvement to the mitigation of outliers in the input activations, where smoothing these values provides more meaningful guidance for pruning.

1182

## C.3 VARIOUS UNSTRUCTURED SPARSITY RATIOS

1184

We established a default unstructured sparsity ratio of 50%. In this section, we investigate the impact of varying sparsity ratios, as detailed in Table 6. For stochRIA, we report the mean average perplexity after three trials. Given that stochRIA has been shown to be stable, with variance examined in Table 1, we omit the variance to focus on performance. Our findings reveal that Wanda is

Table 6: Perplexity on Wikitext-2 with different sparsity.  $\alpha = 1.0$ .

Sparsity	Method	Sampling	L2-7b	L2-13b	L3-8b	OPT-1.3b
Dense	-	-	5.47	4.88	6.14	14.62
50%	Wanda	-	7.79	6.28	10.81	22.19
	RIA	Full	<b>6.88</b>	<b>5.95</b>	<b>9.44</b>	18.94
	stochRIA	10%	6.91	<b>5.95</b>	9.46	<b>18.78</b>
60%	Wanda	-	15.30	9.63	27.55	38.81
	RIA	Full	<b>10.39</b>	<b>7.84</b>	19.52	26.22
	stochRIA	10%	10.62	7.97	<b>19.04</b>	<b>25.93</b>
70%	Wanda	-	214.93	104.97	412.90	231.15
	RIA	Full	<b>68.75</b>	<b>51.96</b>	169.51	98.52
	stochRIA	10%	72.85	62.15	<b>155.34</b>	<b>93.29</b>

particularly sensitive to higher sparsity ratios, whereas both RIA and our proposed stochRIA demonstrate robustness to increased sparsity, maintaining stable performance across a broader range of conditions. Interestingly, we observed that on LLaMA3-8b and OPT1.3b, stochRIA consistently outperforms RIA, whereas on LLaMA2-7b and LLaMA2-13b, the reverse is true. This intriguing phenomenon may be attributed to the heavy noise present in the sampling process for LLaMA3-8b and OPT1.3b. In such cases, selecting a subset of weights through stochRIA may yield more reliable relative weight information, resulting in improved performance.

## D ADDITIONAL EXPERIMENTS

### D.1 IMPLEMENTATION DETAILS

Our selected baselines are implemented using the source code from Wanda<sup>1</sup> and RIA<sup>2</sup>. The default settings remain unchanged to ensure consistency. Notably, we explicitly set the sequence length to 2048 instead of using the maximum possible length to enable a fair comparison, following the strategy outlined in RIA.

The training-free fine-tuning component is based on DSnoT<sup>3</sup>. We configure the maximum cycle count to 50 and set the update threshold to 0.1. The default power of variance for regrowing and pruning is set to 1. Additionally, we incorporate the regularized relative design, resulting in our modified approach, DSnoT.

The seed for sampling the calibration data is set to 0. For N:M structural pruning, to enable an intuitive comparison, we use the standard approach without employing channel reallocation or linear sum assignment, as used in RIA.

### D.2 OPTIMAL $\ell_p$ NORM

In this study, we further explore the influence of the  $\ell_p$  norm, considering standard norms where  $p \in [1, 2, 3, 4]$ , as well as the 0-norm and  $\infty$ -norm. The results are presented in Table 7. We observed that higher  $p$  values degrade performance, as reflected by the perplexity scores, with  $p = 1$  yielding the best results. This may be due to the fact that in pruning, significantly magnifying the differences between weights is not beneficial. Additionally, we found that both the 0-norm and  $\infty$ -norm do not yield promising results, as they capture only partial, and often highly biased, information about the weights.

<sup>1</sup><https://github.com/locuslab/wanda/tree/main>

<sup>2</sup><https://github.com/biomedical-cybernetics/Relative-importance-and-activation-pruning>

<sup>3</sup><https://github.com/zyxxmu/DSnoT>

1242 Table 7: Perplexity scores on Wikitext-2 for  $p$ -norm. The sparsity ratio is 50%, and all results  
 1243 correspond to  $\alpha = 1$ .

p	LlaMA2-7b	LlaMA2-13b	LlaMA3-8b	OPT-1.3b
1	<b>6.88</b>	<b>5.95</b>	<b>9.44</b>	<b>18.95</b>
2	6.90	5.96	9.48	19.02
3	6.95	6.01	9.57	19.66
4	7.12	6.08	9.92	20.77
0	7.78	6.28	10.81	22.17
$\infty$	8.60	6.80	11.28	24.92

### D.3 $\ell_p$ NORM RE-WEIGHTING

In this section, we explore different  $\ell_p$  norm re-weighting strategies. Our default re-weighting approach is defined in Equation (3) and is referred to as S1. Additionally, we investigate alternative strategies, denoted as S2, S3, and S4, as specified below:

$$\begin{aligned} S2 &:= \mathbf{S}_{jk} = |\mathbf{W}_{jk}| / (\|\mathbf{W}_{j:}\|_p + \|\mathbf{W}_{:k}\|_p), \\ S3 &:= \mathbf{S}_{jk} = |\mathbf{W}_{jk}| \cdot (\|\mathbf{W}_{j:}\|_p + \|\mathbf{W}_{:k}\|_p), \\ S4 &:= \mathbf{S}_{jk} = |\mathbf{W}_{jk}| / (\|\mathbf{W}_{j:}\|_p^{-1} + \|\mathbf{W}_{:k}\|_p^{-1}). \end{aligned}$$

The comparative results for these strategies are presented in Table 8. As shown, our default strategy (S1) achieves the best performance, while the alternative designs fail to deliver improvements.

Table 8: Perplexity scores on Wikitext-2 for  $\ell_p$ -norm re-weighting with different strategies. The sparsity ratio is 50%, and all results are computed with  $\alpha = 0.5$  and  $p = 1$ .

Strategy	LLaMA2-7b	LLaMA2-13b	LLaMA3-8b	OPT-1.3b
S1 (default)	6.81	5.83	9.34	18.08
S2	6.99	5.91	9.58	19.01
S3	9.32	6.87	17.31	31.66
S4	14.51	20.78	30.47	53.17

We hypothesize that the performance differences arise due to the relative magnitudes of the terms  $\|\mathbf{W}_{j:}\|_p + \|\mathbf{W}_{:k}\|_p$  and  $\|\mathbf{W}_{j:}\|_p^{-1} + \|\mathbf{W}_{:k}\|_p^{-1}$ . Specifically, we assume that  $\|\mathbf{W}_{j:}\|_p + \|\mathbf{W}_{:k}\|_p$  is typically large, while  $\|\mathbf{W}_{j:}\|_p^{-1} + \|\mathbf{W}_{:k}\|_p^{-1}$  is generally small. Consequently, dividing by the former (S2) or multiplying by the latter (S4) reduces the magnitude of the pruning weights. We will provide statistical evidence to validate this assumption in subsequent sections.

### D.4 INFLUENCE OF SAMPLING RATIOS

In this section, we examine the impact of varying sampling ratios in stochRIA. It is important to note that these ratios are applied over  $\min(b, c)$ , where  $b$  and  $c$  represent the number of rows and columns in each layer, respectively. In Table 9, we can see the performance of stochRIA is generally stable and compares favorably to that of RIA when sampling across entire rows and columns, particularly for  $\beta \geq 0.05$ . At this threshold and above, the performance is robust, occasionally even surpassing less noisy sampling configurations. However, at an extremely low ratio of  $\beta = 0.01$ , there is a significant performance decline. Consequently, we have set  $\beta = 0.1$  as the default setting for our experiments.

1296 Table 10:  $R^2$ -DSnoT Hyperparameter Ablations on LLaMA3-8b. Each row shows the non-default  
 1297 hyperparameter values compared to the best-performing method.

1299	base	setting	$p$	grow relative?	$\gamma_1$	prune relative?	$\gamma_2$	perplexity $\downarrow$
1300	Wanda	best	2	✓	0	✗	0.0001	18.99
1301			$p$	1				19.04
1302			$\infty$					18.99
1303		$\gamma$				0		18.99
1304						0.001		18.99
1305								
1306		relative		✗		✗		19.49
1307				✗		✓		19.25
1308				✓		✓		19.63
1309	RIA	best	2	✗	0	✓	0.001	20.50
1310			$p$	1				25.61
1311			$\infty$					20.51
1312		$\gamma$				0		20.51
1313						0.0001		20.52
1314								
1315		relative		✗		✗		21.33
1316				✓		✗		22.16
1317				✓		✓		22.60

1318 Table 9: Perplexity scores on Wikitext-2 for stochRIA with different sampling ratios. The sparsity  
 1319 ratio is 50%, and all results correspond to  $\alpha = 1$ . We highlight those performance drops over 0.1 as  
 1320 significant.

1322	ratio ( $\beta$ )	LlaMA2-7b	LlaMA2-13b	LlaMA3-8b	OPT-1.3b
1323	1	6.91	5.95	9.45	18.88
1324	0.9	6.91	5.95	9.43	18.87
1325	0.5	6.90	5.95	9.42	18.84
1326	0.1	6.91	5.95	9.46	18.78
1327	0.05	6.91	5.96	9.47	18.91
1328	0.01	6.98	6.00	9.69 <b>-0.24</b>	19.36 <b>-0.48</b>

## 1331 D.5 ANALYSIS OF $R^2$ -DSnoT HYPERPARAMETERS

1333 In Section 3.6, we introduced the equations for our proposed  $R^2$ -DSnoT method, specifically Equation  
 1334 (5) and Equation (6). This method primarily involves three key hyperparameters: the regu-  
 1335 larization penalty  $\gamma_1, \gamma_2$  and the norm type  $p$ . Additionally, we consider whether to apply relative  
 1336 importance reweighting during the growing or pruning phases—or during both. Given the number  
 1337 of hyperparameters, understanding their interactions can be computationally expensive and time-  
 1338 consuming.

1339 To address this complexity, we adopt a systematic approach by performing a random search over 20  
 1340 different combinations of hyperparameter settings. These combinations include:  $p \in \{1, 2, \infty\}$ ,  
 1341  $\gamma_1 \in \{0, 0.0001, 0.001\}$ ,  $\gamma_2 \in \{0, 0.0001, 0.001\}$ , and binary choices for relative reweighting  
 1342 (True/False) during both the growing and pruning phases. For each of the 20 trials on the same  
 1343 model, we identify the best-performing combination and treat its hyperparameters as the "ground  
 1344 truth." We then evaluate the behavior under different scenarios and report the results in Table 10.

1345 Our findings reveal several notable insights:

- 1347 • Norm type  $p$ : The smooth  $\ell_p$ -norm with  $p = 2$  consistently achieves the best performance.  
 1348 Compared to the non-differentiable  $\ell_1$ -norm, which underperforms due to its non-smooth  
 1349 nature, and the  $\ell_\infty$ -norm, which focuses only on the largest values and ignores smaller  
 differences, the  $\ell_p$ -norm with  $p = 2$  balances sensitivity and robustness effectively.

1350

- 1351 • Relative importance reweighting: Applying relative reweighting during either the grow-  
1352 ing or pruning phase improves performance significantly—yielding a 0.5 improvement on  
1353 Wanda and 0.83 on RIA. However, applying reweighting to both phases simultaneously  
1354 leads to substantial performance degradation, with a 0.64 and 2.1 drop on Wanda and RIA,  
1355 respectively.
- 1356 • Regularization penalty  $\gamma$ : The impact of  $\gamma$  is minimal, as variations in its value result in  
1357 only marginal differences in performance. This finding highlights the greater importance  
1358 of the relative reweighting strategy.

1359

1360

1361

1362

1363

1364

1365

1366

1367

1368

1369

1370

1371

1372

1373

1374

1375

1376

1377

1378

1379

1380

1381

1382

1383

1384

1385

1386

1387

1388

1389

1390

1391

1392

1393

1394

1395

1396

1397

1398

1399

1400

1401

1402

1403